

# Parametric Optimization of Biodiesel Fuelled Engine Noise using the Taguchi Method

Satish A. Patil

Mechanical Engineering  
Dr. D. Y. Patil Institute of Technology and  
PDEA's College of Engineering  
Pune, India  
sapcoeh@rediffmail.com

R. R. Arakerimath

Mechanical Engineering  
G H Raisoni College of Engineering and Management and  
Savitribai Phule Pune University  
Pune, India  
rachayya.arakerimath@raisoni.net

**Abstract**—Biodiesel is a renewable, biodegradable, and efficient fuel that can be blended with petro-diesel in any proportion. The noise in the engine resulting from the combustion has a direct effect on the engine's performance. Many studies have examined the engines' vibration and noise when using diesel and biodiesel blends. This study examines the optimization of diesel blends, load, and compression ratio in the aspect of reducing noise on a Kirloskar single-cylinder diesel engine. Noise was measured at the engine and its exhaust on a computerized setup and for different loads. The experimental results showed that a blend with 15% biodiesel, at 7kg load, and 18 compression ratio produced the lowest noise. Moreover, the Taguchi method was utilized, and experimental results were validated by an ANN.

**Keywords**—transesterification; biodiesel; noise; optimization

## I. INTRODUCTION

Any alternative to diesel fuel should be replicable, economical, and technically acceptable [1]. Biodiesel is produced by the transesterification of renewable vegetable oils and animal fats with the use of alcohol. Biodiesel is highly degradable and nontoxic. Meanwhile, it has low emissions of carbon monoxide, particulate matter, and unburned hydrocarbons. Due to these properties, biodiesel has attracted wide attention as a replacement to diesel fuel [1, 2]. Biodiesel can be used without modifications in conventional compression ignition engines. Noise and vibrations are major issues of diesel engines [3, 4]. Engine body vibrations and noise are rich in information about the engine's operating parameters and physical condition [4, 5]. Excess noise and vibrations wear out components such as bearings, grouting, and couplings, increasing maintenance cost due to more component failures and unplanned operations. Due to noise and vibrations' importance, there is a need to study the effect of biodiesel and its blends on engine's life and performance [6-8]. Noise level depends on the load and the blending ratio of biodiesel [5]. As a result, it is necessary to extend an engine's life by using optimal blends, after analyzing their impact in noise [5-9].

## II. EXPERIMENTAL PROCESS

A Kirloskar TV1 VCR single cylinder, four stroke, constant speed, water-cooled diesel engine, having 3.5HP at 1500rpm, was used on a computerized test bed equipped with measuring

instruments such as thermocouples, dynamometer, tachometer and flow meters. The engine's specifications are shown in Table I.

TABLE I. ENGINE'S SPECIFICATIONS

Name	Kirloskar
No. of cylinders	1
No. of strokes	4
Type of cooling	Water cooled
Power developing capacity	3.5kW at 1500rpm
Compression ratio range	12-18
Stroke	110mm
Bore	87.5mm
Cylinder volume	661

Noise levels were measured by a noise meter for four different fuel blends on variable load conditions and compression ratios as per the Taguchi array. The study focused on the input parameters of biodiesel blends for examining the diesel engine's operating conditions. Noise was measured at the engine and its exhaust. A noise meter was placed at 0.5m distance from the engine for measuring its noise, and another was placed outside the room near the exhaust pipe end to measure the noise at the exhaust [3-5]. The noise meter and its specifications are shown in Figure 1 and Table II respectively.

TABLE II. NOISE METER'S SPECIFICATIONS

Display	14mm (0.55") LCD with backlight
Parameter measurement	LP, Lmax, Leq, LN
Frequency range	31.5Hz-8kHz
Measurement range	LP: 30~130dB (A)
Resolution	0.1 dB
Accuracy	±1dB



Fig. 1. Noise meter.

Corresponding author: Satish A. Patil

www.etasr.com

Patil & Arakerimath: Parametric Optimization of Biodiesel Fuelled Engine Noise using Taguchi Method

Four fuel types were tested, namely: B0 consisting of 100% diesel, B15 consisting of 15% biodiesel and 85% diesel, B20 consisting of 20% biodiesel and 80% diesel, and B25 consisting of 25% biodiesel and 75% diesel [2, 3, 9]. Biodiesel blend, load on the engine, and compression ratio were the parameters whose effects on the engine's noise were studied. The parameters' levels are listed in Table III.

TABLE III. PARAMETRIC CONDITIONS

A: Blend	B: Load	C: Compression ratio
A1 = 0	B1 = 0	C1 = 16
A2 = 15	B2 = 4	C2 = 17
A3 = 20	B3 = 7	C3 = 17.5
A4 = 25	B4 = 10	C4 = 18

A. Noise Analysis

The orthogonal array of the input parameters indicates the number of combinations for the experiments. This selection of orthogonal array is based on three parameters and four levels for each parameter [2,5]. The array was obtained by Minitab using the following operating parameters:

Taguchi Design  
 Design Summary  
 Taguchi Array L16(4^3)  
 Factors: 3  
 Runs: 16  
 Columns of L16 (4^5) array: 1 2 3

TABLE IV. SAMPLE READINGS OF TAGUCHI ARRAY FOR PARAMETER OPTIMIZATION

Blend	Load	C.R.	Noise at the engine	Noise at the exhaust	Noise at the engine SNR	Noise at the exhaust SNR
0	0	16	92.75	108.9	-39.3463	-40.7406
0	4	17	93	109.25	-39.3697	-40.7684
15	4	16	93.75	112.15	-39.4394	-40.996
15	7	18	95	110.45	-39.5545	-40.8633
15	10	17.5	95.6	110.95	-39.6092	-40.9025
20	0	17.5	91.7	110.45	-39.2474	-40.8633
25	10	16	96.35	111.9	-39.677	-40.9766

The fourth row of Table IV gives the optimum values of input parameters for noise among the various blends. Signal-to-noise ratio (SNR) measures how the response varies relatively to the nominal or target value under different noise conditions. Depending on the goal, different SNRs may be chosen. In this experiment, lower SNRs are better. Optimal conditions were met with B15 blend, 7kg applied load, and 18 compression ratio, where the noise was 95dB at the engine and 110.45dB at the exhaust.

B. Taguchi Analysis: Noise versus Blend, Load, C.R.

Taguchi method analysis results for noise at the engine versus blend, load, and C.R are shown in Table V, while the regression's resulted equation is:

$$Noise\ at\ the\ engine = 96.6 - 0.0507Blend + 0.371Load - 0.255C.R. \quad (1)$$

TABLE V. NOISE AT THE ENGINE MODEL SUMMARY

S	R-Sq	R-Sq(adj)
0.2196	76.30%	40.76%

Taguchi model's analysis results on noise at the exhaust versus blend, load, and C.R are shown in Table VI, and the regression's resulted equation is:

$$Noise\ at\ the\ exhaust = 107.89 + 0.0518Blend + 0.1900Loads + 0.044C.R. \quad (2)$$

TABLE VI. NOISE AT THE EXHAUST MODEL SUMMARY

S	R-Sq	R-Sq(adj)
0.0658	86.48%	66.21%

C. Validation of Experimental Results by Artificial Neural Network (ANN)

The results of noise at the engine and the exhaust were validated by an ANN. An ANN script, shown in Table VII, was used for obtaining the output from the input parameters.

TABLE VII. ANN CONFIGURATION SCRIPT

clc; close all; clear all;
x = xlsread('Input1');
y = xlsread('Output2');
net = newff(minmax(x),[20,1],{'logsig','purelin','trainlm'});
net.trainparam.epochs = 1000;
net.trainparam.goal = 1e-15; net.trainparam.lr = 0.01;
net = train(net, x, y);
y_net = net(x);
plot(y);hold on; plot(y_net, 'r');
error = (y - y_net);

III. RESULTS AND VALIDATION

A. Noise at the Engine

The experimental results for noise at the engine, the values calculated by the ANN, and the error between them are shown in Table VIII and a comparative graph of these values is shown in Figure 2. Apparently, there is a small difference, less than 1.2%, between the experimental and the ANN calculated values.

TABLE VIII. EXPERIMENTAL AND ANN RESULTS

Blend	Load	C.R.	Noise at the engine	Noise by ANN	Error	Error %
0	7	17.5	97	96	-1	-1.0%
0	10	18	95.2	96	0.8	0.8%
15	7	18	95	96	1	1.0%
20	10	17	95.9	95.5	0	0.0%
25	7	17	94.8	95.6	0.8	0.8%
25	10	16	96.35	95.2	-1.15	-1.2%

The regression plot obtained by the Taguchi model for the experimental results was compared with the ANN regression plot. The regressions' R-square value was around 80%. The straight line in these plots shows that the data fit a normal probability distribution. There are very low residual values, as

all residuals obtained are almost along the line in both plots. The similarity in these plots validates the results.

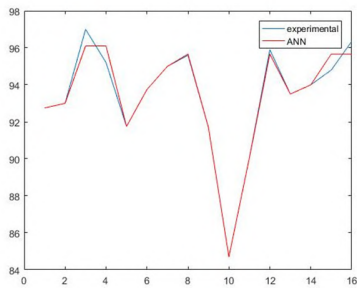


Fig. 2. Comparison of experimental and ANN noise values at the engine.

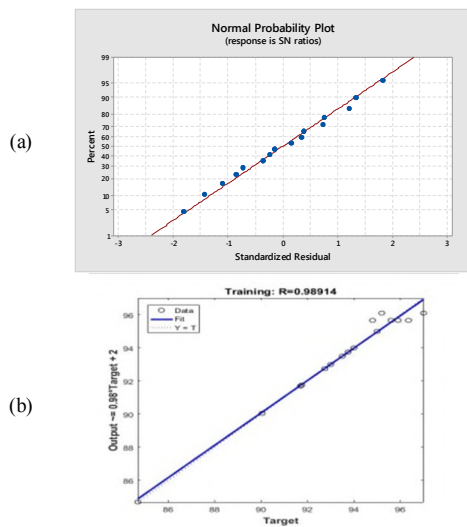


Fig. 3. Residual plot for noise at the engine by (a) Minitab, (b) ANN.

**B. Noise at the Exhaust**

The experimental results of noise at the exhaust, the values calculated by the ANN, and the error between them are given in Table IX. Moreover, a comparative graph of these values is shown in Figure 4. Apparently, there is a tiny difference between experimental and ANN results, less than 0.3%, for noise at the exhaust.

TABLE IX. EXPERIMENTAL AND ANN RESULTS

Blend	Load	C.R.	Noise at the exhaust	Noise byANN	Error	Error %
0	0	16	108.9	109.2	0.3	0.27%
0	4	17	109.25	109.1	-0.15	-0.14%
15	7	18	110.45	110.45	0	0.00%
15	10	17.5	110.95	110.95	0	0.00%
20	0	17.5	110.45	110.45	0	0.00%
25	10	16	111.9	111.9	0	0.00%

After comparing the regression plots of experimental and ANN results in Figures 3 and 5, we can see that there are very few residual values, and all values obtained are almost along the line indicating a normal probability distribution. The regression's R-square value was 86.48%. The similarity in these plots validates the results.

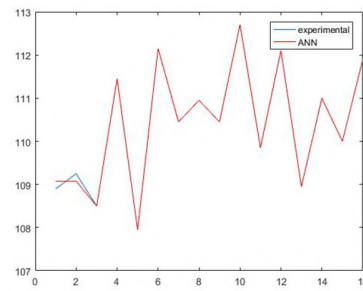


Fig. 4. Comparison of experimental and ANN noise at exhaust.

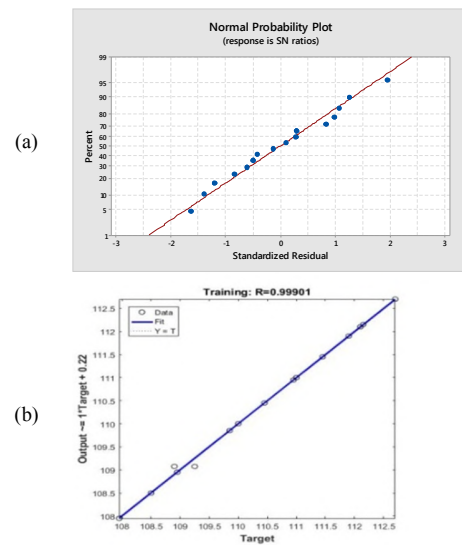


Fig. 5. Residual plot for noise at the exhaust by (a) Minitab, (b) ANN.

**IV. CONCLUSION**

This study examined the optimization of noise reduction at the engine and its exhaust with biodiesel blend, load, and compression ratio of the engine as input parameters. Analysis was carried out utilizing the Taguchi method, and optimization of the input parameters was performed by using SNR [10, 11]. The experimental results obtained by Minitab were validated by an ANN. The main conclusions of this study are:

- Optimal input parameters were: a blend with 15% biodiesel, applied load of 7kg, and compression ratio 18, resulting to 95dB noise at the engine and 110.45dB at its exhaust.
- R-square values obtained by regression analysis were around 80% and more, indicating that the obtained model fits to the actual data.
- There are small to tiny differences between the experimental and the ANN's noise values.
- All regression residuals of both Minitab and ANN were very low and almost along the line in both methods. The similarities in both plots validated the results.

## REFERENCES

- [1] D. Patil and R. Arakerimath, "Performance characteristics and analysis of Jatropha oil in multi-cylinder turbocharge Compression Ignition Engine," *International Journal of Engineering Research and Development*, vol. 1, no. 10, pp. 50–55, Jun. 2012.
- [2] S. A. Patil and R. R. Arakerimath, "Optimization of Biodiesel Synthesis using Heterogeneous Catalyst (SiO<sub>2</sub>) from Karanja Oil by Taguchi Method," *International Journal of Engineering and Advanced Technology*, vol. 9, no. 2, pp. 5597–5600, Dec. 2019.
- [3] A. A. Khaskheli, H. J. Arain, I. A. Memon, U. A. Rajput, and M. J. Ahsan, "Emission and Noise Characteristics of a Diesel Engine Fuelled with Diesel-Chicken Oil Biodiesel Blends," *Engineering, Technology & Applied Science Research*, vol. 10, no. 2, pp. 5387–5391, Apr. 2020.
- [4] S. Saridemir and U. Agbulut, "Combustion, performance, vibration and noise characteristics of cottonseed methyl ester–diesel blends fuelled engine," *Biofuels*, Sep. 2019, doi: 10.1080/17597269.2019.1667658.
- [5] E. Uludamar, E. Tosun, and K. Aydın, "Experimental and regression analysis of noise and vibration of a compression ignition engine fuelled with various biodiesels," *Fuel*, vol. 177, pp. 326–333, Aug. 2016, doi: 10.1016/j.fuel.2016.03.028.
- [6] H. Yıldırım, A. N. Özsezen, and A. Çınar, "Vibration and Noise Depending upon Engine Speed in a Diesel Engine Fueled with Biodiesel," presented at the 6th European Conference on Renewable Energy Systems, Istanbul, Turkey, Jun. 25-27, 2018.
- [7] B. Heidary, S. R. Hassan-beygi, B. Ghobadian, and A. Taghizadeh, "Vibration analysis of a small diesel engine using diesel-biodiesel fuel blends," *Agricultural Engineering International: CIGR Journal*, vol. 15, no. 3, pp. 117–126, Jul. 2013.
- [8] J. A. Grajales, H. F. Quintero, C. A. Romero, and E. Henao, "Engine Diagnosis Based on Vibration Analysis Using Different Fuel Blends | SpringerLink," *Advances in Condition Monitoring of Machinery in Non-Stationary Operations*, vol. 9, pp. 267–274, Sep. 2017.
- [9] K. Sivaramkrishnan and P. Ravikumar, "Performance Optimization of Karanja Biodiesel Engine Using Taguchi Approach and Multiple Regressions," *ARPJ Journal of Engineering and Applied Sciences*, vol. 7, no. 4, pp. 506–516, Apr. 2012.
- [10] S. Jaikumar, S. K. Bhatti, and V. Srinivas, "Emission and vibration characteristics of Niger seed oil biodiesel fueled diesel engine," *Journal of Mechanical Engineering and Sciences*, vol. 13, no. 4, pp. 5862–5874, Dec. 2019, doi: 10.15282/jmes.13.4.2019.11.0467.
- [11] M. M. Etefagh, M. H. Sadeghi, V. Pirouzpanah, and H. Arjmandi Tash, "Knock detection in spark ignition engines by vibration analysis of cylinder block: A parametric modeling approach," *Mechanical Systems and Signal Processing*, vol. 22, no. 6, pp. 1495–1514, Aug. 2008, doi: 10.1016/j.ymssp.2007.11.027.

## AUTHORS PROFILE

**Satish A. Patil** is a research Scholar at the Mechanical Engineering, Dr. D. Y. Patil Institute of Technology (DYBIT), Pune (MS), India, and a Assistant Professor in the Department of Mechanical Engineering, PDEAs College of Engineering, Manjari (Bk), Pune, India. Affiliated to Savitribai Phule Pune University, Pune.

**Rachayya R. Arakerimath** is a Professor and the Head of the Mechanical Engineering Department, Savitribai Phule Pune University, Pune G H Rasoni College of Engineering, Pune, India. He has 24 years of teaching experience and has worked at various levels. He is an approved Ph.D. guide under the Universities of Pune and Nagpur. He has published more than 100 papers in conferences and journals. He is also a reviewer for international journals.

## BRAKE THERMAL EFFICIENCY ANALYSIS OF ENGINE FUELED KARANJA BIODIESEL USING TAGUCHI AND VALIDATION OF RESULTS

SATISH A. PATIL<sup>1\*</sup> & DR. R. R. ARAKERIMATH<sup>2</sup>

<sup>1</sup>Research Scholar, DYPatil Institute of Technology, Pune (MS), India

<sup>2</sup>HOD, Mechanical Engineering, G H Raison College of Engineering and Management, Wagholi, Pune, India

### ABSTRACT

*Biodiesel is synthesized from oils produced from vegetables and fats of animals which have properties like renewability, biodegradability, and as an efficient fuel. It is easily blended with petro diesel at any proportion. Engine noise-generating due to combustion in engines has a direct effect on engine performance. Some researchers are working on the engine using petro diesel and different blends of biodiesel for performance characteristics over the world. This paper covers the study of input parameters optimization for BTH of the engine. The tests have carried out at different combinations as per the orthogonal array obtained by the Taguchi method. This selection of orthogonal array has based on three parameters along with four levels of all individual parameters. The experimental output BTH values calculated have noted by the computerized engine setup. The results obtained by Minitab software have compared with results obtained by ANN and validated.*

**KEYWORDS:** Transesterification, Biodiesel, Brake Thermal Efficiency

**Received:** Jun 08, 2020; **Accepted:** Jun 28, 2020; **Published:** Aug 17, 2020; **Paper Id.:** IJMPERDJUN2020780

### INTRODUCTION

Use of diesel fuels in many different areas and have importance for the wealth of the country, there should be an alternative to diesel. An alternative to diesel fuel should be replicable, economical, as well as technically acceptable [1]. Biodiesel is produced by the transesterification process from renewable oils obtained from vegetable and animal fats using alcohol. Highly degradable, nontoxic, particulate matters, less carbon monoxide emission, unburned hydrocarbons are some important properties of biodiesel. Because of these properties, biodiesel has acquired international focus as a replacement for diesel [2]. Biodiesel may be used without modifications in existing compression ignition engines.

Totally 16 numbers of experiments have done as per array prepared by Minitab software using different inputs such as Biodiesel Blends, Load on Engine, and Compression Ratio. The output BTH of the engine with Karanja oil biodiesel blends for different sets of experiments obtained have noted. For the optimization of input parameters, the results have analyzed using the Taguchi method [3]. The main effective plot and interaction plots have plotted. The input parameter optimal conditions based on SN ratio value have searched for the maximum BTH of the engine [4, 5]. The regression residual plot obtained by Minitab is compared with the regression residual plot by ANN [6]. The comparison of yield obtained by experimentation and ANN has also plotted together. There are very small differences between these values.

## EXPERIMENTAL SETUP

In the experimental setup, Kirloskar makes TV1, Variable CR, and 3.5 HP @ 1500 RPM. The engine's specifications are as below. The computerized system testbed has equipped with all required measuring instruments such as thermocouples, dynamometer, tachometer, flow meters, etc

**Table 1: Engine Specifications**

Make	Kirloskar
No. of Cylinders	1
No. of Strokes	4
Type of Cooling	Water Cooling system
Power Developing Capacity	3.5 kW @ 1500 rpm.
Range of C. R.	12-18
Stroke length	110 mm
Bore dia.	87.5 mm
Cylinder Volume	661

In this work, four different fuels have tested such as B0 (diesel 100%), B15 (85% diesel with 15% biodiesel), B20 (80% diesel with 20% biodiesel), and B25 (75% diesel with 25% biodiesel)

## OPERATING PARAMETRIC CONDITIONS

The effects of different parameters affecting the Transesterification Process have studied as follows.[6]

- Blends of Biodiesel
- Applied load on Engine
- Compression Ratio of engine

The operating parameter values have given below:

**Table 2: Optimizing Parameter Ranges**

A: Blend	B: Load	C: Compression Ratio
A1 = 0	B1 = 0	C1 = 16
A2 = 15	B2 = 4	C2 = 17
A3 = 20	B3 = 7	C3 = 17.5
A4 = 25	B4 = 10	C4 = 18

## ANALYSIS OF BRAKE THERMAL EFFICIENCY BY TAGUCHI METHOD: [6]

### Orthogonal Array

The parametric design giving the number of conditions for all individual experiments in the orthogonal array. This orthogonal array selection has based on three parameters and four levels for the individual parameter as shown in above table number one.

Orthogonal array obtained by Minitab using operating parameters:

Summary of Taguchi Design

Taguchi Array L 16 ( $4^3$ )

No. of factors: 3

No. of runs: 16

Columns of L16 (4<sup>5</sup>) array: 1 2 3

**Table 3: Sample Readings as per Obtained Taguchi Array**

Blend	Load	C.R.	BTH	SNR_BTH
0	0	16	17.49	24.8558
15	4	16	22.33	26.97777
15	7	18	22.52	27.05137
20	0	17.5	15.16	23.61398
25	4	17.5	18.34	25.26799

In the above table 3, the yellowish row gives the higher value of the SN ratio which has indicated optimal input parameter values of engine for maximum BTH. For BTH the value of SN ratio, higher is better. The experimental maximum output value of BTH of the engine with input parameters blends B15, applied load 7 kg, compression ratio 18 has 22.52 %.

**TAGUCHI ANALYSIS: BTH VERSUS BLEND, LOAD, C.R.**

**Model Summary**

S	R-Square value	R-Square. (adjusted)
0.6207	91.39%	78.47%

**Regression Equation**

$$BTH = 23.1 - 0.0872 \text{ Blend} + 0.210 \text{ Load} - 0.216 \text{ C.R.} \dots\dots\dots(1)$$

**Main Effective Plot for BTH**

The Plots obtained by Minitab software have shown below

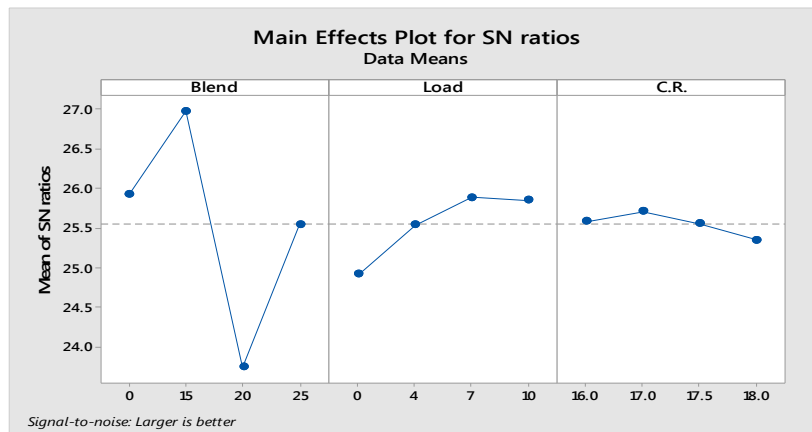


**Figure 1: Main Effect Plot for BTH.**

In the above main effect plots, S/N ratios vs blend, and S/N ratios vs load are comparatively steeper than CR plot. So, blend and load have affected more on the values of BTH. Therefore the effect of remaining one i.e. CR has neglected for further studies in the interaction plot.

**INTERACTION PLOT FOR BTH: (6)**

Generally, the Taguchi method concrete on the main effects and that’s important to test the other interactions. The variations of BTH of engine separately with the effect of blend and load simultaneously have shown in these interaction plots. From this interaction plot, Blend 15 having a larger value of SN ratio at 7kg loads.

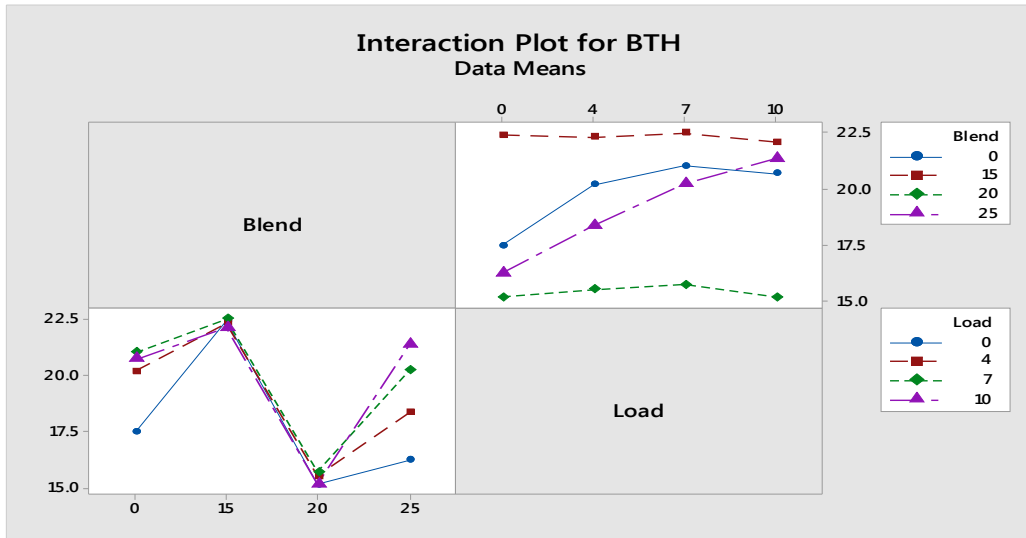


**Figure 2: Interaction Plot for BTH.**

**VALIDATION OF EXPERIMENTAL RESULTS USING TAGUCHI FOR BTH OF ENGINE BY ARTIFICIAL NEURAL NETWORK (ANN)**

Here the experimental results of BTH of the engine have validated by ANN (Artificial Neural Network).

**ANN Script for the Analysis Performed**

Script has written for obtaining the output by putting the values of input parameters

**Table 3: ANN Script for the Analysis Performed**

```

clc; close all; clear all;
x = xlsread('Input1');
y = xlsread('Output2');
net = newff(minmax(x),[20,1],{'logsig','purelin','trainlm'});
net.trainparam.epochs=1000;
net.trainparam.goal=1e-15;
net.trainparam.lr=0.01;
net = train(net, x, y);
y_net = net(x);
plot(y);hold on; plot(y_net, 'r');
error = (y - y_net);
    
```

**Comparison of BTH of Engine Obtained by Experimentation and ANN**

Experimental values of BTH of engine and values calculated by ANN, error between them, and % error are given in table 4.

**Table 4: Sample Readings by Experiment and ANN**

Blend	Load	C.R.	BTH by Exp.	BTH by ANN	Error	Error %
0	0	16	17.49	17.49	0.00	0.00%
15	4	16	22.33	22.33	0.00	0.00%
15	7	18	22.52	22.52	0.00	0.00%
20	10	17	15.15	15.15	0.00	0.00%
25	0	18	16.23	16.23	0.00	0.00%

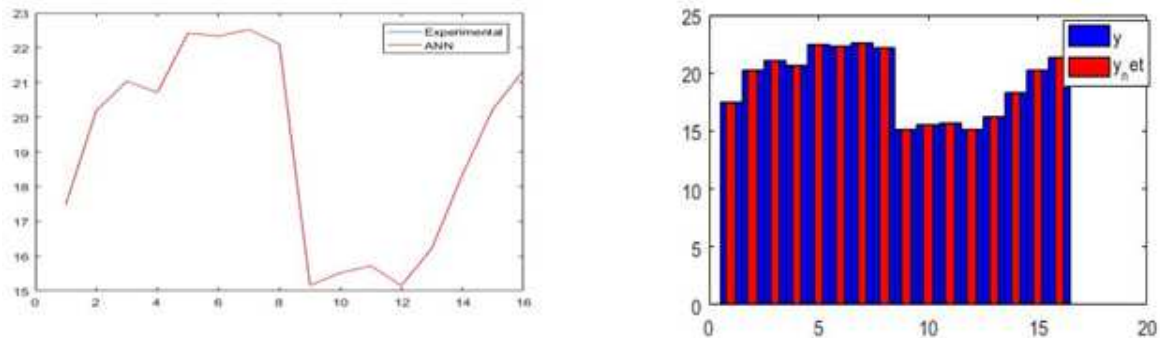


**Figure 3: Comparison of BTH Obtained by Experimentation and ANN.**

The comparative study of BTH of engine obtained by experimentation and ANN is as shown in Figure Fig. (3). There is a zero error in between these two values of BTH of the engine. In the table (3) the all values of BTH of engine obtained by experimentation and by ANN are given. There is no difference between these values and the % error is also zero.

**Regression Plots: (6)**

The regression plots obtained by Minitab software and ANN have shown below. The comparison has made between these plots.

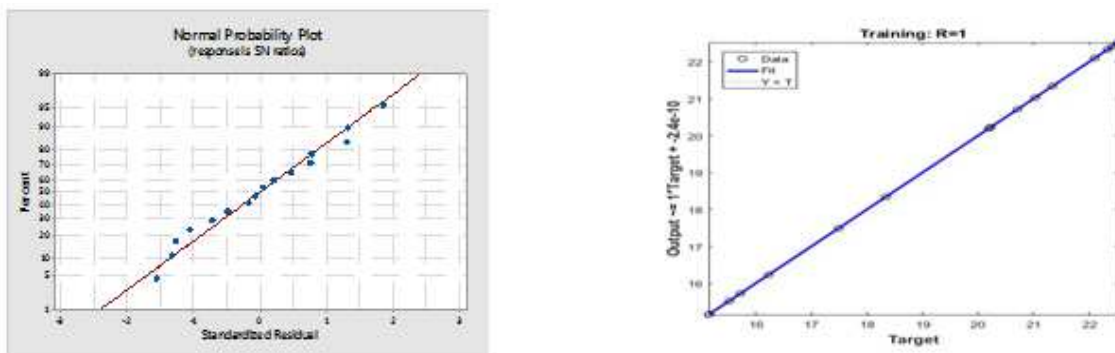


**Figure 4: Comparison between Residual Plot for BTH by Minitab and by ANN.**

There are very low residuals in the above both plots and all readings obtained are nearby or on the straight line. The R-square value for this regression has 91.39%.

## CONCLUSIONS

This work has carried out for optimization of input parameters such as Biodiesel Blend, Load on Engine, and C R for output of BTH of the engine. The Taguchi method analysis using SNR base has performed for the optimization of input parameters. The results obtained by experimentation with Minitab are validated by ANN (Artificial Neural Network). The conclusions are as follows;

- The experimental output BTH of the engine has 22.52 % with optimal input parameters blend B15, applied load 7 kg, and compression ratio 18.
- Interaction plots have shown the variation of BTH of the engine with the effect of blend and load simultaneously and also BTH of the engine has maximum value for blend 15 and load 7 kg.
- The R square value obtained by analysis has 91.39%, shows generated model has fitted to actual given data.
- There have no differences between values of BTH of engine obtained by experimentation and by ANN.
- The regression residuals plot obtained by Minitab has similar to ANN regression plot. Hence results have validated.

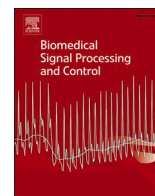
## REFERENCES

1. Dipak Patil, Dr. Rachayya. Arakerimath. *Performance characteristics and analysis of Jatropha oil in multi-cylinder turbocharge Compression Ignition Engine. International Journal of Engineering Research and Development* ISSN: 2278-067X, Volume 1, Issue 10 (June 2012), PP.50-55
2. Kumar, M. Naveen, Sriram. Venkatesh, and M. Manzoor Hussain. "Experimental investigation on influence of process parameters in selective laser sintering on roundness using taguchi method." *International Journal of Mechanical and Production Engineering Research and Development* 7.6 (2017): 45-52.
3. Avinash1, Kailash B Anwar2 & Gowreesh, *Optimization Of Diesel Engine Parameters with Blend of Pongamia Biodiesel and Diesel Using Taguchi Method, International Journal of Applied Engineering Research and Development (IJAERD) ISSN(P): 2250-1584; ISSN(E): 2278-9383 Vol. 5, Issue 1, Feb 2015, 13-20*
4. Matheswaran, M., and P. Suresh. "Study of EDM Process Parameters of Surface Roughness in Titanium Using Taguchi Method." *International Journal of Mechanical and Production Engineering Research and Development (IJMPERD)* 4.2 (2014): 63-68.
5. Dhruv V. Patel, Tushar M. Patel, Gaurav P Rathod, *Parametric Optimization of Single Cylinder Diesel Engine for Jatropha Biodiesel and Diesel Blend For Brake Specific Fuel Consumption Using Taguchi Method, IOSR Journal Of Mechanical And Civil Engineering (IOSR-JMCE) E-ISSN: 2278-1684, P-ISSN: 2320-334X, Volume 12, Issue 2 Ver. VI (Mar - Apr. 2015), PP 66-72 DOI: 10.9790/1684-12266672*
6. Sivaraman, B. "Optimization of grinding parameters in austenitic stainless steel AISI 317L using taguchi method." *International Journal of Mechanical and Production Engineering Research and Development* 8.2 (2018): 1033-1038.
7. P. Shanmugasundaram Palanisamy, *Performance of Single Cylinder CI Engine Using Blends Of Rubber Seed Biodiesel – Taguchi method U.P.B. Sci. Bull., Series D, Issn 1454-2358, Vol. 76, Iss. 4, 2014.*

8. Chavan S. B., Kumbhar R. R. and Sharma Y. C. , *Transesterification of Citrullus Colocynthis (Thumba) Oil Optimization for Biodiesel Production, Advances in Applied Science Research, 5(3):10-20, 2014.*
9. Alavala, Chennakesava R. "Effect of Temperature, Strain Rate and Coefficient of Friction on Deep Drawing Process of 6061 Aluminum Alloy." *International Journal of Mechanical Engineering 5.6 (2016): 11-24.*
10. Satish A. Patil, R. R. Arakerimath, *Optimization of Biodiesel Synthesis using Heterogeneous Catalyst (SiO<sub>2</sub>) from Karanja Oil by Taguchi Method. International Journal of Engineering and Advanced Technology (IJEAT). ISSN: 2249 – 8958, Volume-9 Issue-2, December 2019.*







## Classification and analysis of cardiac arrhythmia based on incremental support vector regression on IOT platform

S.T. Sanamdikar<sup>a,b,c,d,\*</sup>, S.T. Hamde<sup>a,b</sup>, V.G. Asutkar<sup>a,b</sup>

<sup>a</sup> Department of Instrumentation Engineering, Shri Guru Gobind Singhji Institute of Engineering and Technology, Nanded, India

<sup>b</sup> Swami Ramanand Teerth Marathwada University, Nanded, Maharashtra, India

<sup>c</sup> Department of Instrumentation and Control, PDEA College of Engineering, Manjari Budruk, Pune, India

<sup>d</sup> Savitribai Phule Pune University, Pune, Maharashtra, India

### ARTICLE INFO

#### Keywords:

Discrete wavelet transform  
Higher order statistics  
Incremental support vector regression  
Internet of things  
Cardiovascular disease

### ABSTRACT

The electrocardiogram (ECG) is a diagnostic device capable of monitoring normal or irregular heart function. The entire ECG beat can be categorized into five different forms of beat arrhythmias (N, S, V, F, U). Quick and precise diagnosis of forms of arrhythmia is critical for identifying the heart problem and provides the proper treatment to the patient. In this paper, Discrete Wavelet Transform and Higher Order Statistics techniques has been used for analyzing and determining the ECG signals and implement it on an IOT-based platform. This system is based on three categories: The first approach involves inputting the ECG data; the second approach involves extracting the ECG beats with their respective amplitude from the base line. Wavelet transform function, and higher order statistics are used to eliminate noise and unwanted signal components and thus to extract ECG features. The third approach is to classify the ECG beats based on the Incremental Support vector regression classifier. After classification ECG beat is transmitted to the controller section for signal processing are given to controller section (Arduino Uno). The process can be implemented by employing the statistical feature for the feature extraction from the ECG signal. Compared to other approaches, the method provided by Incremental Support vector regression to identify the ECG beats and predict arrhythmia can provide successful detection of arrhythmias. The basic concept of the proposed system is to provide patients with reliable health care by using cloud data compliance to allow doctors to use this information and to provide a fast and feasible service. The findings show that the proposed algorithm is successful in predicting cardiac arrhythmias, with a 98% that is higher than other approaches.

### 1. Introduction

Recognition of the ECG signal is very crucial in understanding the functioning of the heart as well as the diagnosis of heart disease under different circumstances. The American Heart Association stated in 2006 that 70 million people around the world face the cardiovascular disease problem. The basic reasons for Cardiovascular Disease (CVD) are hypertension, lacking physical exercise, ineffectively adjusted eating regimen, smoking and unusual glucose levels. Because of the existence of noise and heartbeat abnormality, physicians face complications in the Arrhythmias analysis [1,2]. In addition, visual inspection alone can result in a misdiagnosis or irrelevant detection of arrhythmias. Therefore, the computer aided analysis of ECG data supports physicians to proficiently detect arrhythmia. Arrhythmia is a cardiovascular condition

that is caused by abnormal heart activity; electrocardiogram (ECG) is used to detect heart defects. Feature Extraction, selection and classification Construction are the three main steps in the detection of arrhythmias. The ECG beat classification [3] as per ANSI/AAMI EC57:1998 standard database shown in Table 1. In Feature extraction process the input data is transform into different of features for detecting heart diseases. The Purpose of this study is to evaluate the ECG beats classification performance with integrating two methods for feature extraction and evaluation using wavelet transformation and higher order statistics. The evaluation of ECG beats classification performance can be improved by using the incremental support vector regression.

The numerous models of different kinds of feature extraction from ECG signals were achieved in previous studies, and a classification technique was proposed. Feature extraction may contain the non-linear,

\* Corresponding author.

E-mail address: [sanamdikar123@gmail.com](mailto:sanamdikar123@gmail.com) (S.T. Sanamdikar).

**Table 1**

MIT-BIH arrhythmia beats classification per ANSI/AAMI EC57:1998 standard database [21–41].

AAMI classes	MIT-BIH heartbeat classes
Non-Ectopic Beat (N)	Normal Beat (N) Left Bundle Branch Block (LBBB) Right Bundle Branch Block (RBBB) Nodal Escape (j) Atrial Escape Beat (e)
Supra-Ventricular ectopic Beat (S)	Aberrated Atrial Premature Beat (A) Atrial Premature (a) Supraventricular premature (S) Nodal premature (J)
Ventricular ectopic Beat (V)	Ventricular Escape (V) Premature ventricular contraction (E)
Fusion Beat (F)	Fusion of ventricular and normal (F)
Unknown Beat (U)	Unclassifiable (U) paced (p) Fusion of paced and normal (f)

time, frequency domain and multi domain feature extraction [3,4]. For the classification classical methods is used such as Artificial Network, Support Vector Machine (SVM), Super vector regression (SVR) etc. The ECG signal can be easily identified by the noise in the time domain and has a low accuracy level [5,6]. Another approach for extracting the ECG feature based on convolutional neural network model. The model has two sections; the first part extract the feature from ECG signals and second part perform the classification of feature based on the first section. Feature extraction was discussed based on principle component analysis to reduce the multidimensional data and input is processed by three pooling layer approach [7]. These signals cannot be considered as the accurate parameter of ECG signals for accomplishing high arrangement correctness. There are various combinations of methods proposed for classification of the ECG feature extraction. The genetic algorithm and SVM-based classifier designated for the classification of ECG waveforms [8–24] are used for the function optimization. The Extreme learning machine algorithm calculates the minimum weight Single Hidden Layer Feed Forward Neural Network for classification [9]. In the recent study, echo state network was implemented based on the morphology for classifying the normal and abnormal ECG signals of heart. The classification is based on the two classes SVEB and VEB [10]. The extraction of features from non-linear method in the time and space domain based on the T complexity is applied to the RR and 13 different classes are used for classification [11,12].

Although the above mentioned techniques or methods of classification have good results, they used a combined space, time, frequency, linear and non-linear domain for beat classification of the ECG. This research suggests an ECG waveform detection model that extracts multi-domain features based on empirical mode of decomposition with linear discriminatory analysis [13,14]. The combined approach of polyhedral conic separation and k-means clustering was applied as classifier to differentiate the ECG waveforms with 5 different classes such as N for Normal, RBBB for Right Bundle Branch Block, LBBB for Left Bundle Branch Block, APC for Atrial Premature Contraction and VPC for Ventricular Premature Contraction [15–18]. Ref [19] proposed a new cloud based model for automatic classification of ECG beats with minimum processing of signals. HOS and DWT is used for classify the ECG beats based on multivariate analysis [20–23]. The classification is performed based on feed forward neural network machine learning technique and particle swarm optimization [22] An effective method to classify the ECG signal based on the support vector regression analysis on 400 samples of data set of various arrhythmias was proposed [24,25]. The KPCA-SVR approach was used for detecting the cardiac arrhythmia [35]. The proposed model is evaluated and compared with the different techniques of neural network classifiers, and found that it offers better accuracy than the current method.

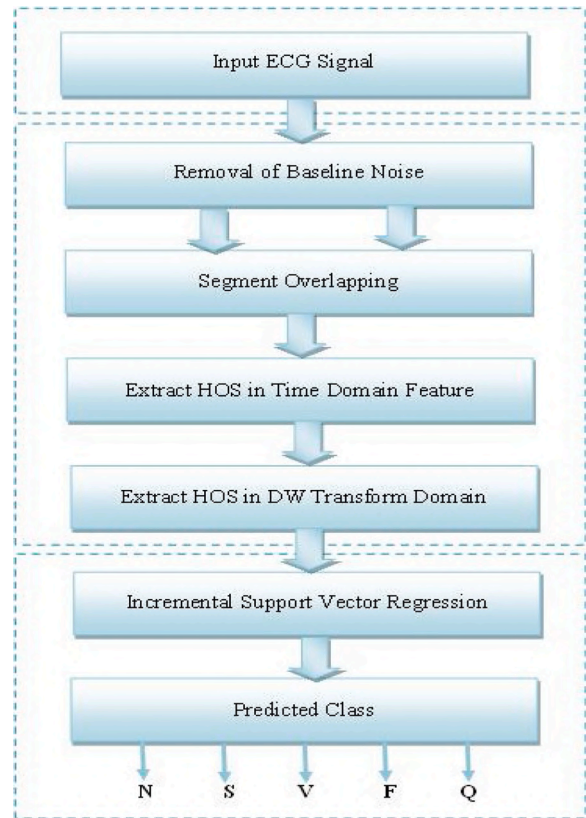


**Fig. 1.** The three tier architecture for recognition and classification of ECG signal for cardiac arrhythmia system.

## 2. Proposed methodology

**Fig. 1** shows the three tier architecture of research work. The System consists of three sections such as input ECG signal, feature extraction and classification. The ECG beats are derived using the discrete wavelet transform and higher order statistics. These non-linear techniques have been used to extract the ECG beats better than others because of their versatility. In the Discrete Wavelet Transform and higher order statistics, the original ECG signal is decomposed in the time domain to remove the low-frequency component to eliminate the baseline and eliminate the high-frequency component to remove the noise and extract the function in the ECG signals. Sample frequency of ECG signal is 360 Hz. In the final step, classification is carried out on the extracted function of ECG beats and decides normal and abnormal arrhythmia activities. After classification of ECG beats sent to the IOT cloud. It is suitable for  $24 \times 7$  monitoring of the patient. In almost all cases, the classification accuracy achieved is above 98%. The key purpose of the new scheme is to provide patients with safer and more effective services by creating a registry of collective records so that practitioners and physicians can use this database to provide evidence and an effective cure for arrhythmia. The execution times we acquired from actualizing the application on the ATMEGA328 P Microcontroller demonstrate that the ECG investigation and characterization can be performed progressively. TCP/IP protocol is used to transfer the data from controller section to remote hospital. Basically two steps for designing a programming logic one for receiving the signal and another is transmitting the signal using TCP/IP protocol. Set an integer number to packet data; be certain that the information is sent without misfortune of data. Heart beat is never transmitted to the base station (Controller) when heart beat is normal. Where the irregular condition is found. The transmitter is turned on and transmits data about heart beat to remote hospital.

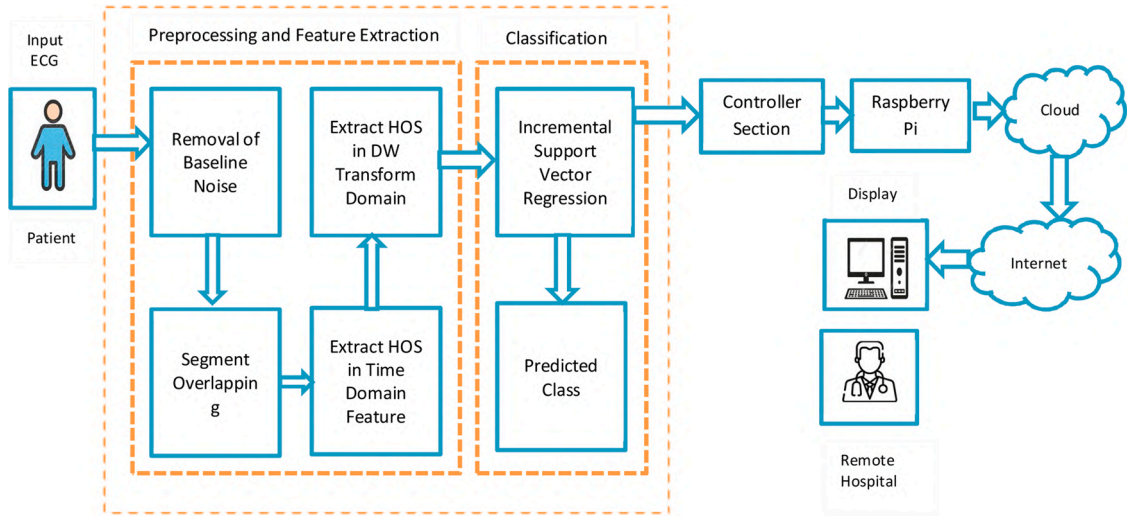


Fig. 2. Complete architecture of proposed model with IOT Platform.

## 2.1. Signal preprocessing

### 2.1.1. Removal of baseline noise

Baseline signal noise has an effect on normal ECG [2]. Noise frequency from around 0.5 to 0.6 Hz. Used high pass filter with the cut-off frequency 0.5 to 0.6 Hz [3,4] to eliminate such noise in signal. If the physical activity of the patient's body increases, then the frequency parameter of the baseline [26–28] increases such that the baseline noise signal is a low signal and a high pass filter with a cut-off frequency of 0.5 to 0.6 Hz is used to eliminate the baseline noise in the ECG signal.

### 2.1.2. Discrete wavelet transform function

In ECG signals consists of variety signals i.e. noise and it is required to remove the undesirable signals and extract useful feature from ECG. So many researchers have developed effective techniques for extracting the important feature for EEG and ECG signals based on the wavelet transform. In this section we will discuss the discrete wavelet transform function in time domain feature with the respective signal shape.

For the feature extraction, we acquire the concept of Yakup Kutlu and Damla Kuntalp [36] studied the wavelet and HOS techniques for noise removal. They proposed the good techniques for noise removal which gives the better result of noise removal as compare to others [27].

The signal is divided into the two parts High and Low frequencies.

The Low frequency again divided into two parts high and low frequency. This process is continued until the signal has been entirely decomposed.

$$y_{\text{high}}[n] = \sum_{k=-\infty}^{\infty} x[k]h[2n+1-k] \quad (1)$$

$$y_{\text{low}}[n] = \sum_{k=-\infty}^{\infty} x[k]g[2n-k] \quad (2)$$

Where,

$x[k]$  is input ECG signal

$g[n]$  and  $h[n]$  is Impulse response of high pass filter

There is  $n+1$  possibility to encrypt ECG signal for the  $n$  level decomposition. Noise is removed from ECG signal using low and high pass filter. In wavelet transformation, approximate precise coefficient is just like binary tree. Such decomposition is applied on low and high frequencies. And again create next level of tree, make  $2^{2n-1}$  in various way to encrypt the ECG signal. Each  $n$  level, there is  $2^{n-1}$  nodes. The wavelet decomposition can be obtained at fourth level that means data in fourth level is used to extract the feature.

### 2.1.3. Higher order statistics

The higher order statistics (HOS) has importance in bio-medical signal processing field but first and second order statistics are not sufficient for all the representing it. So that we used third and fourth order statistics for analysis.

### 2.1.4. Statistical features

For evaluating the feature decomposition of signal is an important step in signal processing. In our proposed scheme we are evaluating some statistical feature such as energy, mean, median, entropy, standard deviation, skewness, kurtosis, covariance and to create feature set [29, 30]. The entire feature is evaluated in MATLAB software. Following are the standard equations used for evaluating feature based on  $C_{ab}$  at 4th level of decomposition

Following features are a set of statistical parameters to measure a distribution,

$$\text{Energy} = \sum_{i=1}^n C_{ab}^2 \quad (3)$$

Standard Deviation

$$\sigma = \sqrt{\frac{1}{N} \sum_{i=1}^N (x_i - \mu)^2} \quad (4)$$

Mean

$$M = \frac{1}{N} \sum_{i=1}^{N-1} A_i \quad (5)$$

2.1.4.1. Kurtosis. used to measure the data sharpness is peaked from ECG signal. In data set  $A_1, A_2, A_n$

$$KUR = \frac{\sum_{i=1}^n (A_i - \bar{A})}{N} / SD^4 \quad (6)$$

Where,  $\bar{A}$ -mean,  $N$ -number of data points,  $SD$ -standard deviation  
Skewness

$$SK = \frac{\epsilon(C_{ab} - \mu a)^3}{\sigma_a^3} \quad (7)$$

The coefficients  $C_{ab}$  is the decomposition coefficient. Here  $i = 1, 2, \dots, i$  is the node number at 4th level of decomposition.  $N$  is the number of coefficients at the coefficients  $C_{ab}$  is the decomposition coefficient. Here  $i = 1, 2, \dots, i$  is the node number at 4th level of decomposition.  $N$  is the

number of coefficients.

### 2.1.5. RR interval features

We have picked RR interim data as the main time space includes in our investigation. Two RR interims are figured straightforwardly from the R areas named as past RR and post RR interims. Past RR is characterized as the time remove among present and past R area while post RR is the time separate between current R area and the accompanying one [31].

- Past RR, (RR<sub>i</sub>): The interval between *i*th R beat and past R beat.
- Post RR RR<sub>(i+1)</sub>: interval between *i*th R beat to next R beat.
- Average of RR interval in 1-min, (RR<sub>1</sub>): Averaged RR interval of 1-min of ECG
- Average 20-min RR interval, (RR<sub>20</sub>): average RR interval of 20-min ECG

## 3. ECG beat classification model

This section describes the ISVR classifier used for the ECG beats classification.

### 3.1. ISVR classifier

The Incremental Support Vector Regression (ISVR) utilizes indistinguishable working standards from the SVM for grouping, with just a couple of minor contrasts. As a matter of first importance, since yield is a genuine number it turns out to be extremely hard to anticipate the current data, which has vast prospects. On account of relapse, an edge of resistance (epsilon) is set in estimate to the SVM which would have just mentioned from the issue. In any case, other than this reality, there is additionally an increasingly confused explanation; the calculation is progressively entangled subsequently to be taken in thought. In any case, the primary thought is consistently the equivalent: to limit mistake, individualizing the hyper plane which expands the edge, remembering that piece of the blunder is endured [32]. In this research Incremental SVR approach is used to develop the regression model. The training data are delivered to adjust the proposed model parameters, at the same time as the take a look at data are used to evaluating the prediction accuracy of the proposed model.

The complete description of ISVR techniques are given below.

- (1) Load the data set.
- (2) Data set can be placed in multi-dimensional function space and the data can be determined based on kernel function.
- (3) To search the linear relationship of data in multi-dimensional space to find another hyper-plan with large vector.

Primarily, ISVR select the hyper-plan with maximum vector value between plan and both positive/negative points. Selection of Optimal hyper-plan is based on distance between data points and hyper-plan is maximum known as support vector.

Given training data set  $(a_1, b_1), \dots, (a_n, b_n), p_i \in \{-1, 1\}$  So we required to learn optimal hyper-plan  $w \cdot a + y = 0$ , with max margin equivalent to decision function  $f(x) = \text{sign}(w \cdot a + y)$

The objective function,  
Max

$$\emptyset(w) = \frac{1}{2} \|w\|^2 \rightarrow \min \quad (8)$$

ST constraint

$$p_i (w^t \cdot a_i) \geq 1, \quad i = 1, 2, \dots, N \quad (9)$$

The above Eq. (10) can be change into optimization problem so that can be solved by Lagrange multiplier technique.

$$\begin{cases} L(w, y, \alpha) = \frac{1}{2} \|w\|^2 - \sum_{i=1}^N \alpha_i (p_i (w \cdot a_i + y) - 1) \rightarrow \min_{w, y} \max_{\alpha} \\ \alpha_i \geq 0, \quad i = 1, 2, 3, \dots, N \end{cases} \quad (10)$$

Apply partial derivatives with respect to *w* and *y* and we will get,

$$\begin{cases} \frac{\partial}{\partial w} L(w, y, \alpha) = 0 \Rightarrow w = \sum_{i=1}^N \alpha_i p_i a_i \\ \frac{\partial}{\partial y} L(w, y, \alpha) = 0 \Rightarrow \sum_{i=1}^N \alpha_i p_i \end{cases} \quad (11)$$

Adding Eq. (12) into Eq. (11) and removes the variables *w* and *y* and we get dual optimization problem

$$\begin{cases} Q(\alpha) = \sum_{i=1}^N \alpha_i - \frac{1}{2} \sum_{i=1}^N \sum_{j=1}^N \alpha_i \alpha_j p_i p_j a_i \cdot a_j \rightarrow \max_{\alpha} \\ \alpha_i \geq 0 \quad \forall i = 1, \dots, N \text{ and } \sum_{i=1}^N \alpha_i p_i \end{cases} \quad (12)$$

If input data is not linearly distinguishable, to find min. value,

$$\emptyset(w) = \frac{1}{2} w^t \cdot w + C \sum_{i=1}^N \xi_i \rightarrow \min_{w, y, \xi} \quad (13)$$

$\xi$  is slack variable It can be used for classification error and also minimized. C is user defined penalty variable. Final function is as follows;

$$w = \sum_{i=1}^k \alpha_i p_i a_i \quad (14)$$

It also written as,

$$f(x) = \text{sign} \left( \sum_{i=0}^N \alpha_i p_i (a^t \cdot a_i) + y \right) \quad (15)$$

The Eq. (16) shows the dot product two variables known as training and testing data set. Presents the kernel function to integrate the sample data with proposed mapping function [39]. Final function can be written as,

$$\begin{aligned} f(x) &= \text{sign} \left( \sum_{i=0}^N \alpha_i p_i \emptyset(a^t) \cdot \emptyset(a_i) + y \right) \\ &= \text{sign} \left( \sum_{i=0}^N \alpha_i y_i F(a^t a_i) + b \right) \end{aligned} \quad (16)$$

The Eq. (17) shows the kernel function  $F(a^t a_i)$ . Our kernel function for proposed ISVR technique is as follows;

$$F(a^t a_i) = \exp(-\gamma \|a^t - a_i\|^2) \quad (17)$$

Above Eq. (17) will be used in proposed classification which has better classification accuracy.

To determine the performance of proposed model of ISVR classifier six parameters are used which is Sensitivity, Specificity, Accuracy, false positive rate, false negative rate and precision. All the parameters are calculated as follows.

$$\text{Sensitivity} = \frac{T\_P}{(T\_P + F\_N)} \quad (18)$$

**Table 2**  
Classify the MIT/BIH arrhythmia dataset into training sets.

Beat	Class	Records	Total
N	N	100, 101, 103, 105	400
S	SVP	109, 111, 207, 214	400
V	PVC	118, 124, 212, 231	400
F	VFN	106, 119, 200, 203	400
Q	FPN	209, 222	200
<b>Total</b>			<b>1800</b>

$$Specificity = \frac{T_N}{(T_N + F_P)} \tag{19}$$

$$Accuracy = (T_P + T_N) / (T_P + F_P + T_N + F_N) \tag{20}$$

$$FAR = (F_P) / (F_P + T_N) \tag{21}$$

$$FRR = (F_N) / (T_P + F_N) \tag{22}$$

$$Precision = (T_P) / (T_P + F_P) \tag{23}$$

Where, T\_P is for the True Positive, T\_N is for True Negative, F\_N is for False Negative, F\_P is for False positive, FAR is for false positive rate and FRR is for false negative rate.

#### 4. IOT platform

In Fig. 2, display the complete system architecture but in this section it presents the functioning of IOT in the framework proposed.

##### 4.1. Hardware used

###### 4.1.1. Data acquisition

The ECG signal is integrated with the circuit and used to amplify and filter ECG signal. CE 8232 is used for data acquisition connected to Arduino of ADC pins with 2.0 V to 3.5 V operational voltage.

###### 4.1.2. Raspberry pi

The small sized raspberry pi is used with high specification in our

proposed IOT based model. It has a core processor 32 bit 40 pin Quad with speed of 900 MHz. It has 4 USB port, 1 GB of memory (RAM), Ethernet port, and micro-SD port to store the OS and other files, and 5 V, 2A to run low power consumption.

###### 4.1.3. Arduino uno

microcontroller with 16 MHz clock frequency, 14 I/O pins, USB Port, and power supply. It has 10-bit ADC to digitize the ECG signals and transfer to Raspberry pi with sample rate 860 sps (samples per second). The Inter-Integrated Circuit (I2C) protocol is used for data transfer.

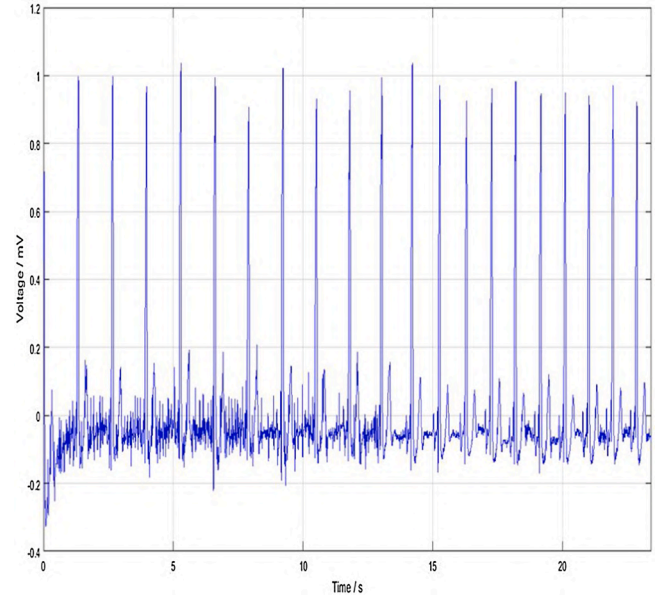


Fig. 4. Supra-ventricular premature ECG sample.

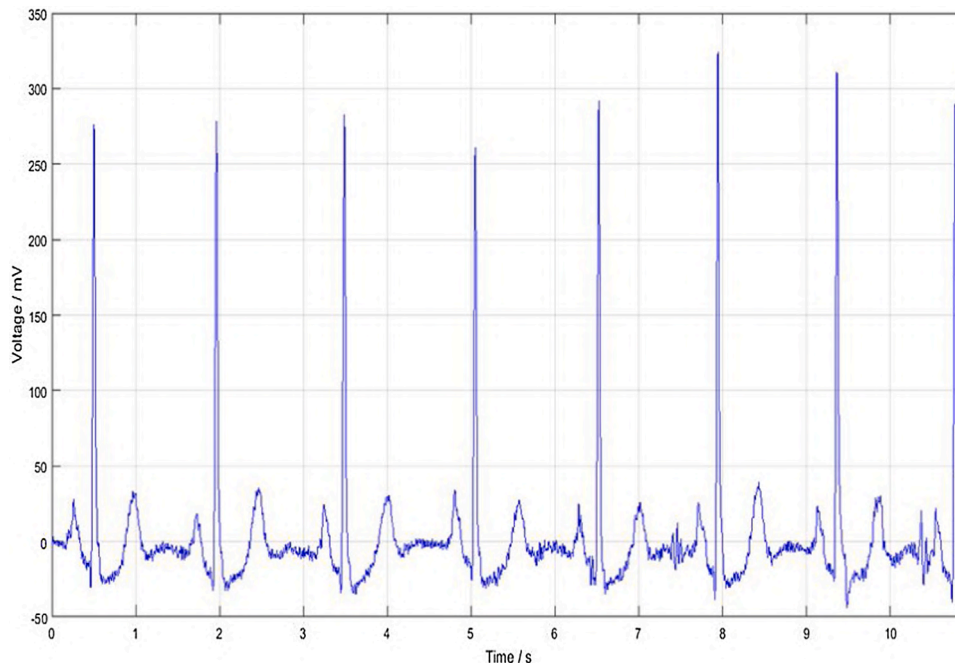


Fig. 3. Normal ECG sample.

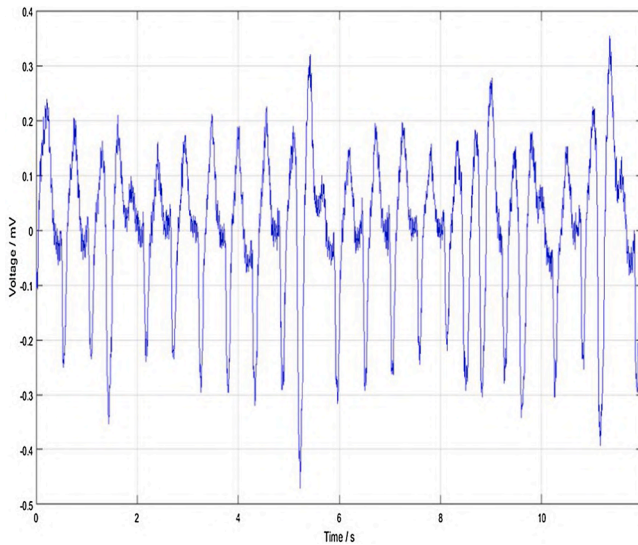


Fig. 5. Premature ventricular contraction ECG Sample.

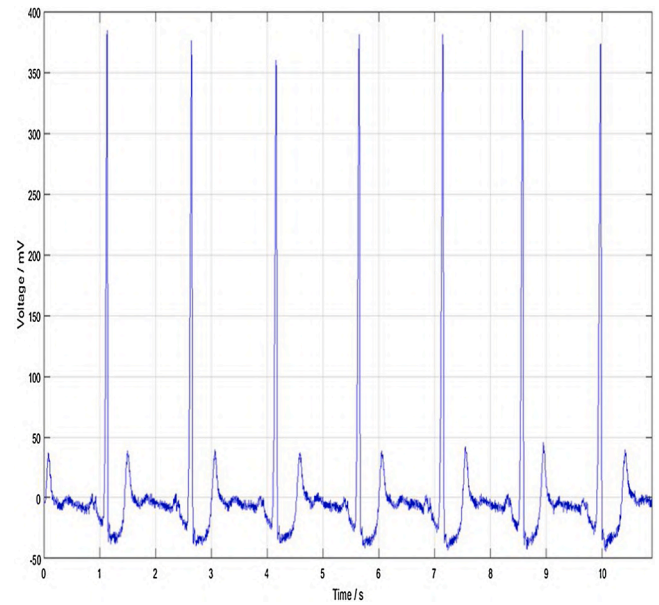


Fig. 7. Fusion of paced and normal ECG sample.

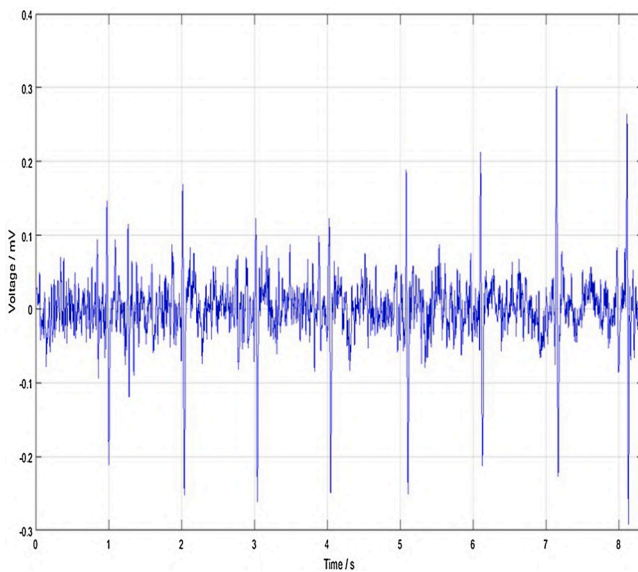


Fig. 6. Fusion of ventricular and normal ECG sample.

#### 4.2. Controller section

In this section, the signals coming from the signal processing section are given to controller section (Arduino Uno). Arduino Uno has been used for converting analog signal to digital signal [33,34]. The data is coming from the sensor and sent to Raspberry from Arduino Uno. For the internet connectivity, Wi-Fi Modem is connected to the Raspberry Pi and data is stored to the cloud as the Raspberry Pi is registered to the cloud [36–38].

#### 4.3. IOT cloud

The ECG signals are the transition of Wi-Fi linked to the Raspberry Pi from Raspberry Pi into the cloud. Data authorization, identity procedure has been ensured in such a way that the most effective authorized character would have access to the data of the person concerned [32]. ECG beats can be plotted for remote hospital doctor to view processing section.

## 5. Result analysis

The proposed method characterizes the five different classes ECG beat annotations:

- N - Normal
- S - Supraventricular Ectopic Beats
- V - Ventricular Ectopic beats
- F - Fusion of ventricular and normal
- Q - Fusion of Paced and Normal

In this Experimental analysis, the MIT/BIH arrhythmia dataset is utilized for validate the proposed Method. The database contains comment for both planning data and beat class data checked by free specialists. This dataset to create a five different beats categories in according to the Association for the advancement of Medical Instrumentation (AAMI) [21–41]. The Table 1 represents the summary of mapping beat classification per ANSI/AAMI EC57:1998 standard database. The Complete MIT-BIH arrhythmia dataset has been classified into 1800 samples of training sets as shown in Table 2.

Table 2 shows the record. Each record has unique number and this number shows the specific set of characteristics of ECG [40]. N class for 400 samples is obtained from 100, 101, 103 and 105 records. For APC class, 400 samples are obtained from 109, 111, 207 and 214 records. For VFN class, 400 samples of are obtained from 118, 124, 212 and 231 records. For PVC class, 400 samples are obtained from 106, 119, 200 and 203 records. Finally, for FPN class 200 samples are obtained from 209 and 222 records.

Following the sampling and pre-processing of ECG signals a complete of 1800 samples of ECG beats is needed. It is proposed that each ECG beat be grouped into the five heartbeats accompanying it composes: N S, V F, and Q beats.

#### 5.1. N: normal

From Fig. 3, ECG signals we extract Time and Frequency based features. Those features are classified using ISVR.

##### 5.1.1. S-Beat

Supraventricular untimely beats speak to untimely actuation of the atria from a site other than the sinus hub and can begin from the atria or the atrio ventricular hub (called junctional untimely beats), however by far most are atrial in cause.

**Table 3**  
Performance analysis of ECG beats.

Class	Accuracy	Sensitivity	Specificity	FAR	FRR	Precision
N-Normal	0.984000	0.92	0.988571	0.005747	0.148148	0.92
S-SVP	0.986667	0.88	0.994286	0.008547	0.083333	0.88
V-PVC	0.989333	0.88	0.997143	0.008523	0.043478	0.88
F-VFN	0.986667	0.88	0.994286	0.008547	0.083333	0.88
Q-FPN	0.986667	0.88	0.994286	0.008547	0.083333	0.88

**Table 4**  
Time domain feature.

Class	F1 Mean	F2 Variance	F3 Std. deviation	F4 Skewness	F5 Kurtosis	F6 Inst amplitude	F7 Range	F8 Modulated amplitude	F9 Max freq	F10 RR interval
N-Normal	0.00070	1283.5	35.826	5.0614	33.494	0.0290	777.01	4.17e+08	1189.10	257.87
S-SVP	0.00153	4458.62	66.772	3.4610	18.043	0.0237	624.14	1.45E+09	7635.45	344.37
V-PVC	0.00037	1080.72	32.874	1.7510	10.391	0.0062	354.19	3.51E+08	4162.32	260.62
F-VFN	4.7E-05	4072.35	63.814	4.0384	24.124	0.0059	985.05	1.32E+09	3688.40	270.00
Q-FPN	0.00120	10189.7	100.94	3.9727	22.174	0.2092	1333.90	3.31E+09	11400.3	259.62

Fig. 4 shows the Supra-Ventricular Premature signal to extract the Time and frequency based feature and classify those feature using ISVR.

#### 5.1.2. V-Beat

Premature ventricular complexes/contractions (PVCs; also referred to a premature ventricular beats, premature ventricular depolarization, or ventricular extra systoles) are triggered from the ventricular myocardium in a variety of situations. PVCs are common and occur in a broad spectrum of the population. Premature Ventricular Contraction ECG sample from combined dataset is shown Fig. 5.

Fig. 5 shows the Premature ventricular contraction signal to extract the Time and frequency based feature and classify those feature using ISVR.

#### 5.1.3. F: Fusion of ventricular and normal

A fusion beat occurs at the point when electrical driving forces from various sources follow up on a similar area of the heart simultaneously. In the event that it follows up on the ventricular chambers it is known as a ventricular combination beat, while impacting flows in the atrial chambers produce atrial combination beats.

Fig. 6 shows the Fusion of Ventricular and Normal signal to extract the Time and frequency based feature and classify those feature using ISVR.

#### 5.1.4. Q: fusion of paced and normal

A pacemaker combination beat happens when the natural beat and pacemaker improvement beat somewhat depolarize the ventricles a hybrid QRS complex.

Fig. 7 shows the Fusion of Paced and Normal signal to extract the Time and frequency based feature and classify those feature using ISVR.

### 5.2. Performance analysis classes

Table 3 shows the comparing performance of ECG beats based on proposed ISVR method. The result shows that specificity, sensitivity, positive prediction and false prediction rate of arrhythmia detection obtained better results by the suggested method. While accuracy measures the overall system performance over the selected classes of beats, the other metrics are specific to each class and they measure the ability of the classification algorithm.

### 5.3. Time domain feature vector

Table 4 shows estimate the various feature of ECG beats in time domain vector.

### 5.4. Frequency domain feature vector

Table 5 shows estimate the various feature of ECG beats in frequency domain vector.

In this investigation observed in other useful fields i.e. Incremental SVR based on the Wavelet transform and HOS as compared to various classifiers that deal with feature space of large dimensionality. The Table 6 shows the various classifier accuracies result with the proposed ISVR classifier. The overall accuracies achieved with the proposed ISVR classifier are equal to 98%. This result is better than those achieved by the GSNN, KPCA-SVR and SVM. Comparison of the proposed systems built in this research with similar systems work in literature is a tedious task because each author used different methods of classification, types of arrhythmia, classification of arrhythmia, types of dataset and system performance. Fig. 8 demonstrates the comparative study of the method proposed with other classifier techniques. All the techniques for the classification were working well. The best performance of accuracy in classification is calculated using an ISVR method [35,42].

## 6. Discussion

A few investigations have tended to this issue by presenting various strategies. Berdakh Abibullaev et al. (2010) has recognized an approach for detection and classification of cardiac arrhythmias based on SVM but this research work has indicated less accuracy as compare to our proposed scheme with regards to the classification of cardiovascular arrhythmias except if they are constrained in light of the utilization of SVM. Miquel Alfaras et al. (2019) propose a technique for fast ECG arrhythmia classification based on machine learning from MIT-BIH database used for classification but has not applicable to real-time application. Yakup Kutlu et al. (2012) describes feature extraction based on the HOS and wavelet transforms techniques. The performance accuracy is measured based on the sensitivity, specificity and selectivity of 90%, 92% and 98% respectively. But the outcomes show up extremely constrained contrasted with the professional requirements for arrhythmia recognition. This Stage our work doesn't have impediments in examined information presented a statistical features and the created symptomatic methodology has a few favorable circumstances in contrast with past works.

The feature extraction mechanism is proposed to extract the effective features for ECG recognition and to implement for continuous patient monitoring on the IOT-based platform. The ECG data is sampled from the MIT-BIH arrhythmia dataset and the data is pre-processed with cut-off frequency using high pass filter. The various features for classifying ECG beats have been proposed in the literature. The classification

**Table 5**  
Frequency domain feature.

Class	F11 Wavelet Mean	F12 Wavelet Variance	F13 Std. deviation	F14 Wavelet Skew	F15 Wavelet Kurtosis	F16 Inst amplitude	F17 Wave Range	F18 Modulated amplitude	F19 Max freq	F20 Wavelet Energy
N-Normal	0.1800	7924.70	89.020	0.9939	15.320	1.03e-06	1063.9	1.63e+08	330.71	3.7e+09
S-SVP	0.0015	4458.62	66.77295	3.4610	18.04385	0.02379	624.1	1.45E+09	7635.45	344.375
V-PVC	0.4413	5004.94	70.745	0.2638	12.098	2.18E-08	781.6	1.01E+08	329.30	2.2E+09
F-VFN	0.2552	11438.50	106.95	0.4824	17.456	3.83E-07	1404.4	2.34E+08	621.01	5.5E+09
Q-FPN	0.1998	41872.10	204.62	0.2503	16.141	5.42E-08	2360.8	8.41E+08	1860.10	2.2E+10

**Table 6**  
Accuracy of different classifier.

Class	ISVR	SVM	GSNN	KPCA-SVR
N-Normal	98.4000	95.4167	98.2200	97.4000
S-SVP	98.6667	94.1667	96.3300	96.1300
V-PVC	98.9333	94.5833	98.2100	97.9300
F-VFN	98.6667	94.5833	97.2400	97.9600
Q-FPN	98.6667	94.5833	98.2300	93.9300

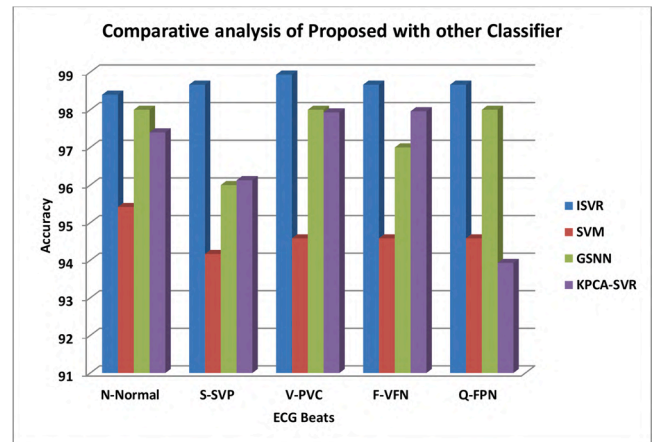


**Fig. 8.** Graphical representation of proposed ISVR classifier with other classifier.

performance of ECG beats depends on the extraction of features, the reduction of features and the algorithm for classification. As the results obtained clearly indicate, ECG beats classification technique based on Incremental SVR feature extraction to improve accuracy, sensitivity, specificity and precision. This improvement may be caused by good Incremental SVR classifier performance.

**7. Conclusion**

In this paper the Incremental support vector regression based on wavelet and HOS can be effectively applied and to achieve a reasonable degree of accuracy for the detection of cardiac arrhythmia. An efficient Incremental Support Vector Regression based ECG classification system is proposed to carry out automatic ECG arrhythmia detection by classify the patient’s ECG into corresponding five kinds of cardiac arrhythmia condition such as Normal, Supraventricular Ectopic, Ventricular Ectopic, Fusion of ventricular and normal and Fusion of Paced and Normal beats and implement it on an IOT based embedded platform. For pre-processing the ECG signal, the high pass filter with the cut-off frequency 0.5 to 0.6 Hz is used and the noise interference is reduced. The proposed model uses the cardiac arrhythmia dataset MIT-BIT for the classification of the ECG signals. ISVR classifier efficiency is calculated by their accuracy, sensitivity, specificity, False Positive Rate, False Negative Rate and Precision. We also estimate some statistical feature in time and frequency domain. The findings show that the proposed algorithm is successful in predicting cardiac arrhythmias, with a 98% that is higher than other approaches. The basic idea of the proposed framework is to give patients better and better welfare administrations by executing cloud system data with the goal that the specialists use this information and provide a quick and productive solution.

**Financial and ethical disclosures**

This work is not supported fully or partially by any funding organization or agency.

## Credit author statement

This research paper is written, implemented, designed software and hardware etc are done by all three authors equally. we are all three responsible for this paper.

## Declaration of Competing Interest

The authors declare that they have no known competing financial interests or personal relationships that could have appeared to influence the work reported in this paper.

## Appendix A. Supplementary data

Supplementary material related to this article can be found, in the online version, at <https://doi.org/10.1016/j.bspc.2020.102324>.

## References

- [1] Berdakh Abibullaev, Won-Seok Kang, Seung Hyun Lee, Jinung an, Classification of cardiac arrhythmias using biorthogonal wavelets and support vector machines, *Int. J. Adv. Comput. Technol.* 2 (June (2)) (2010).
- [2] Padmavathi Kora, K. Sri Rama Krishna, ECG based heart arrhythmia detection using wavelet coherence and Bat algorithm, *Sensing Imaging* 17 (June (1)) (2016).
- [3] Gustavo Lenis, Nicolas Pilia, Axel Loewe, Walther H.W. Schulze, Olaf Dössel, Comparison of baseline wander removal techniques considering the preservation of ST changes in the ischemic ECG: a simulation study, *Comput. Math. Methods Med.* (2017), 9295029, <https://doi.org/10.1155/2017/9295029>. Hindawi. 13 pages.
- [4] N. Maglaveras, T. Stamkopoulos, K. Diamantaras, C. Pappas, M. Strintzis, ECG pattern recognition and classification using nonlinear transformations and neural networks: a review, *Int. J. Med. Inform.* 52 (1998) 191–208.
- [5] Hongqiang Li, Danyang Yuan, Youxi Wang, Dianyin Cui, Lu Cao, Arrhythmia classification based on multi-domain feature extraction for an ECG recognition system, *Sensors* 2016 (16) (2016) 1744, <https://doi.org/10.3390/s16101744>.
- [6] R. Rodríguez, A. Mexicanob, J. Bilac, S. Cervantesd, R. Ponceb, Feature extraction of electrocardiogram signals by applying adaptive threshold and principal component analysis, *J. Appl. Res. Technol.* 13 (2015) (2015) 261–269.
- [7] Carlos Lastre-Dom-nguez, Yuriy S. Shmaliy, Oscar Ibarra-Manzano, Jorge Munoz-Minjares, Luis J. Morales-Mendoza, ECG signal denoising and features extraction using unbiased FIR smoothing, *BioMed Res. Int.* 2019 (2019), 2608547, <https://doi.org/10.1155/2019/2608547>. Hindawi. 16 pages.
- [8] M. Ashtiyani, S. Navaei Lavasani, A. Asgharzadeh Alvar, M.R. Deevband, Heart rate variability classification using support vector machine and genetic algorithm, *J. Biomed. Phys. Eng.* (2018) 423–434.
- [9] M. Zubair, J. Kim, C. Yoon, An automated ECG beat classification system using convolutional neural networks, in: 6th International Conference on IT Convergence and Security (ICITCS), Prague, 2016, pp. 1–5, <https://doi.org/10.1109/ICITCS.2016.7740310>.
- [10] V. Bhagyalakshmi, R.V. Pujeri, Geetha D. Devanagavi, GB-SVNN: genetic BAT assisted support vector neural network for arrhythmia classification using ECG signals, *J. King Saud Univ. - Comput. Inf. Sci.* (2018).
- [11] Jinkwon Kim, Hang Sik Shin, Kwangsoo Shin, MyoungHo Lee, Robust algorithm for arrhythmia classification in ECG using extreme learning machine, *Biomed. Eng. Online* (2009), October.
- [12] Alessandro Scirè, Fabrizio Tropeano, Aris Anagnostopoulos, Ioannis Chatzigiannakis, Fog-computing-Based heartbeat detection and arrhythmia classification using machine learning, *Algorithms* 2019 (12) (2019) 32, <https://doi.org/10.3390/a12020032>.
- [13] Miquel Alfaras, Miguel C. Soriano, Silvia Ortín, A fast machine learning model for ECG-Based heartbeat classification and arrhythmia detection", *Front. Phys.* 7 (July) (2019), 103.
- [14] S. Karimifard, A. Ahmadian, Morphological heart arrhythmia classification using hermitian model of Higher-order statistics, in: 29th Annual International Conference of the IEEE Engineering in Medicine and Biology Society, Lyon, 2007, pp. 3132–3135, <https://doi.org/10.1109/IEMBS.2007.4352993>.
- [15] D. Arotaritei, H. Costin, C. Rotariu, A. Pasarica, Cardiac arrhythmia classification using T-complexity measure, in: International Conference and Exposition on Electrical and Power Engineering (EPE), Iasi, 2016, pp. 431–434, <https://doi.org/10.1109/ICEPE.2016.7781377>.
- [16] E. Izci, M.A. Ozdemir, R. Sadighzadeh, A. Akan, Arrhythmia detection on ECG signals by using empirical Mode decomposition, in: Medical Technologies National Congress (TIPTKNO), Magusa, 2018, pp. 1–4, <https://doi.org/10.1109/TIPTKNO.2018.8597094>.
- [17] O. Perlman, Y. Zigel, G. Amit, A. Katz, Cardiac arrhythmia classification in 12-lead ECG using synthetic atrial activity signal, *IEEE 27th Convention of Electrical and Electronics Engineers in Israel, Eilat* (2012) 1–4, <https://doi.org/10.1109/IEEE.2012.6376901>.
- [18] E. Cimen, G. Ozturk, Arrhythmia classification via k-means based polyhedral conic functions algorithm, in: International Conference on Computational Science and Computational Intelligence (CSCI), Las Vegas, NV, 2016, pp. 798–802, <https://doi.org/10.1109/CSCI.2016.0155>.
- [19] J.M. Lillo-Castellano, et al., Symmetrical compression distance for arrhythmia discrimination in cloud-based big-data services, *IEEE J. Biomed. Health Inform.* 19 (July (4)) (2015) 1253–1263, <https://doi.org/10.1109/JBHI.2015.2412175>.
- [20] fish 0.punct]" > Thripurna Thatipelli, Padmavathi Kora, Electrocardiogram beat classification using Discrete Wavelet Transform, higher order statistics and multivariate analysis, *Int. J. Eng. Technol. (IRJET)* 04 (July (07)) (2017) 854–858.
- [21] A. for the Advancement of Medical Instrumentation, et al., Testing and Reporting Performance Results of Cardiac Rhythm and ST Segment Measurement Algorithms, *ANSI/AAMI EC38*, vol. 1998, 1998.
- [22] Shweta H. Jambukia, Vipul K. Dabhi, Harshadkumar B. Prajapati, ECG beat classification using machine learning techniques, *Int. J. Biomed. Eng. Technol.* 26 (1) (2018) 32–53.
- [23] Roshan Joy Martis, U. Rajendra Acharya, K.M. Mandana, A.K. Ray, Chandan Chakraborty, Application of principal component analysis to ECG signals for automated diagnosis of cardiac health, *Expert Syst. Appl.* 39 (2012) 11792–11800.
- [24] Farhana Akter Mou, Muhammed Abdullah Al Mahmud, A.H.M. Zaidul Karim, Salma Nazia Rahman, Shaikh Rashedur Rahman, Classification of electrocardiogram signal using support vector machine based on fractal extraction by FD, *Am. J. Circuits Syst. Signal Process.* 3 (3) (2017) 12–22.
- [25] S.T. Sanamdikar, S.T. Hamde, V.G. Asutkar, Machine vision approach for arrhythmia classification using incremental super vector regression, *J. Signal Process.* 5 (2) (2019) 1–8, <https://doi.org/10.5281/zenodo.2637567>.
- [26] Rahul Kher, Signal processing techniques for removing noise from ECG signals, *J. Biomed. Eng.* 1 (2019) 1–9.
- [27] Yurong Luo, Rosalyn H. Hargraves, Ashwin Belle, Ou Bai, Xuguang Qi, Kevin R. Ward, Michael Paul Pfaffenberger, Kayvan Najarian, A hierarchical method for removal of baseline drift from biomedical signals: application in ECG analysis, Hindawi Publishing Corporation, *Scientific World J.* (2013), 896056, <https://doi.org/10.1155/2013/896056>, 10 pages.
- [28] Anurag Trivedi Harimohanrai, Shailja Shukla, ECG signal processing for abnormalities using multi-resolution wavelet transform and artificial neural network classifier, in: Deptt of Electrical Engg, Jabalpur Engineering College, Jabalpur, MP, India, 2020.
- [29] Tanya Kambo, Ram Avtarjaswal, De-noising and statistical feature extraction of the ecg signal using wavelet analysis, *Int. J. Electr. Electron. Data Commun.* 4 (September (9)) (2016).
- [30] Mingfeng Jiang, Yaming Wang, Ling Xia, Feng Liu, Shanshan Jiang, Wenqing Huang, The combination of self-organizing feature maps and support vector regression for solving the inverse ECG problem, *Comput. Math. Appl.* 66 (10) (2013) 1981–1990, <https://doi.org/10.1016/j.camwa.2013.09.010>. ISSN 0898-1221.
- [31] Chun-Cheng Lin, Chun-Min Yang, Heartbeat Classification Using Normalized RR Intervals and Morphological Features, *Mathematical Problems in Engineering*, 2014, pp. 1–11, <https://doi.org/10.1155/2014/712474>.
- [32] D. Azariadi, V. Tsoutsouras, S. Xydis, D. Soudris, ECG signal analysis and arrhythmia detection on IoT wearable medical devices, in: 2016 5th International Conference on Modern Circuits and Systems Technologies (MOCASST), Thessaloniki, 2016, pp. 1–4, <https://doi.org/10.1109/MOCASST.2016.7495143>.
- [33] P. Singh, A. Jasuja, IoT based low-cost distant patient ECG monitoring system, in: 2017 International Conference on Computing, Communication and Automation (ICCCA), Greater Noida, 2017, pp. 1330–1334, <https://doi.org/10.1109/ICCCA.2017.8230003>.
- [34] M.F. Amri, M.I. Rizqyawan, A. Turnip, ECG signal processing using offline-wavelet transform method based on ECG-IoT device, in: 2016 3rd International Conference on Information Technology, Computer, and Electrical Engineering (ICITACEE), Semarang, 2016, pp. 1–6, <https://doi.org/10.1109/ICITACEE.2016.7892404>.
- [35] S.T. Sanamdikar, S.T. Hamde, V.G. Asutkar, Cardiac arrhythmia detection on electrocardiogram beats based on KPCA and SVR, *Int. J. Emerg. Technol. Learn.* 11 (2) (2020) 44–51.
- [36] Yakup Kutlu, Damla Kuntalp, Feature extraction for ECG heartbeats using higher order statistics of WPD coefficients, *Comput. Methods Programs Biomed.* 105 (2015) 257–267.
- [37] Junaid Ahmed Zubairi, Abdul Rahman Alahdal, Muhammad Arshad Malik, IoT-based ambulatory vital signs data transfer system, *J. Comput. Netw. Commun.* 2018 (2018), 4071474, <https://doi.org/10.1155/2018/4071474>, 8 pages.
- [38] M. Raeiatibanadkooki, S.R. Quachani, M. Khalilzade, K. Bahaadinbeigy, Real time processing and transferring ECG signal by a mobile phone, *Acta Inform. Med.* 22 (6) (2014) 389–392, <https://doi.org/10.5455/aim.2014.22.389-392>.
- [39] V. Vapnik, *Statistical Learning Theory*, Wiley, Chichester, GB, 1998.
- [40] <https://www.physionet.org/content/mitdb/1.0.0/>.
- [41] G.B. Moody, R.G. Mark, The impact of the MIT-BIH arrhythmia database, *IEEE Eng. Med. Biol.* 20 (May-June (3)) (2001) 45–50, <https://doi.org/10.1109/51.932724> (PMID: 11446209).
- [42] S.T. Sanamdikar, S.T. Hamde, V.G. Asutkar, Analysis and classification of cardiac arrhythmia based on general sparsed neural network of, *SN Appl. Sci.* 2 (7) (2020), 1244, <https://doi.org/10.1007/s42452-020-3058-8>.

# Monogenic Wavelet Phase Encoded Descriptors for Brain Tumor Image Detection

Deepak O. Patil  
Department of Instrumentation  
SGGS Institute of Engineering and  
Technology  
Nanded, Maharashtra, India  
dopatil25@gmail.com

Satish T Hamde  
Department of Instrumentation  
SGGS Institute of Engineering and  
Technology  
Nanded, Maharashtra, India  
sthamde@sggs.ac.in

**Abstract**— Brain tumor has a low survival rate and also affect a patient's social life. Early detection and further treatment of the abnormal growth of mass is a significant step during treatment to restrict the progression. MR image screening by the medical expert is a time-consuming and tedious task. This paper presents the development of computer-aided tool to detect brain tumor images. The proposed algorithm employs monogenic wavelet phase-encoded features for tumor detection. Phase component of the monogenic wavelet efficiently extracts the structural information from the input magnetic resonance images. The dimensionality of CLBP textural descriptors extracted from the phase component is further reduced using neighborhood component analysis feature selection. Finally, the support vector machine classifies the test magnetic resonance image as healthy or abnormal. The proposed approach is evaluated using two popular MR imaging databases and simulation results show enhanced performance compared to other existing algorithms.

**Keywords**— Brain tumor detection Monogenic wavelet phase encoding Neighborhood component analysis, CLBP features.

## I. INTRODUCTION

Different medical imaging plays a significant role to detect and classify brain tumors. Magnetic resonance imaging (MRI) is a popular choice by the medical practitioners for identifying brain abnormalities. Although, other types of modalities are also available and used for a diagnosis like computer tomography (CT) and positron emission tomography (PET) imaging. Brain diagnosis problems are primarily addressed using the MR imaging type. Recent studies are focused on application image processing algorithms for automatic detection and classification of brain tumors in different categories like benign and malignant.

In India, 5 to 10 individuals out of 100,000 are suffering from CNS brain tumors and about 40% caners spread to the brain [1]. Brain tumor has a low survival rate and affects seriously on patients social and professional life. The Brain tumor is abnormal growth which creates a mass in the brain portion. Early detection of abnormal growth of a tissue mass is critical for the diagnosis and patient treatment. Manual analysis of magnetic resonance images is laborious and subjective. So, MR imaging-based computer based automatic detection and classification algorithms for tumor detection has been proposed [2].

In this paper, a monogenic wavelet phase-encoded texture descriptor-based technique for brain tumor image detection is proposed. The algorithm classifies an input magnetic resonance image as normal or cancerous. In the first step, the input MR image is pre-processed to remove the noise and further enhanced by applying filtering techniques before monogenic wavelet signal analysis. During the second step, filtered and enhanced image is

applied to monogenic wavelet signal analysis and phase component is extracted. The third step involves the extraction of Completed local binary pattern (CLBP) texture descriptors from all the sub-bands of the monogenic wavelet phase component.

In the fourth step, neighbourhood component analysis (NCA) feature selection is employed to choose the most relevant and to discard redundant features thereby reducing the feature vector dimensionality. NCA is a filter technique to select the most powerful features from a large pool of input features. Finally, a healthy or abnormal MR image decision is done using the support vector machine (SVM) classifier. The algorithm is validated using two most widely used and publicly available databases: (a) e-health laboratory dataset and (b) Harvard medical laboratory dataset. The proposed algorithm evaluation is presented in terms of sensitivity, specificity, precision, accuracy, and F1-score.

The paper is organized as follows. Recent brain tumor detection in MR images techniques are briefed in section II. The proposed brain tumor detection method using monogenic wavelet phase encoding is presented in section III. Section IV explains monogenic wavelet analysis, CLBP descriptor and NCA feature selection approach in brief. Experimental results are presented in section V. Finally, section VI concludes the article.

## II. PRIOR WORK

A variety of approaches are developed for abnormal brain tumor image detection by researchers in the last two decades. Multiresolution analysis methods using discrete wavelet transform (DWT), shearlet and curvelet transform for capturing abnormal signatures from the MR images are proposed in [3]. Particle swarm optimization (PSO) based feature selection approach is employed and the optimal feature set is classified by SVM classifier attaining 97.38% classification rate. The input image is first filtered using Weiner filter and local binary pattern (LBP), and Gabor wavelet transform (GWT) features are extracted in [4].

A generative progressive growing GAN along with the convolutional neural network (CNN) is combined for brain tumor image detection in [5]. Enhanced performance is obtained with data augmentation technique resulting in 91.08% detection accuracy using the deep learning framework. Geometrical and shape features like local ternary (LT) and quinary patterns (LQ) are extracted for brain tumor detection in [6]. SVM and k-nearest neighbor (KNN) classifiers achieved 97.5% detection accuracy using parabola descriptors. Distinct regions are obtained from the magnetic resonance images by utilizing k-means clustering technique and textural features are extracted in [7]. Finally, the artificial neural network (ANN) based classification

achieved 94.07% accuracy. Post-processing enhancement strategy is employed in the work to enhance the accuracy rate.

After segmenting the enhanced image by implementing binomial mean and other statistical parameters, geometric and textural descriptors are extracted from the input MR images for tumor detection is developed in [8]. The Genetic Algorithm (GA) based feature selection algorithm is used to select the discriminating features and fed to SVM classifier resulting in 90% classification rate. In [9], the input MR image is first decomposed using DWT and only high-energy sub-band is selected. High variance descriptors are then extracted from this sub-band and fed to ANN for the classification producing the detection rate of 99.7%.

Abnormal tissue detection and analysis algorithm using partial differential diffusion-filter (PDDF) and a combination of LBP and CLBP are illustrated in [10]. The proposed algorithm distinguishes tumor and healthy MR images with 96.6% accuracy. Input MR images are divided into various slices first, then Adaptive Convex-Region Contour (ACRC) algorithm and SVM classifier are employed for normal or abnormal brain image in [11]. 2D image slices are reconstructed into 3D form for better visualization in the work. The difficulty of low detection accuracy because of low contrast and non-illumination MR images is addressed in [12]. In the proposed method, input MR images are first enhanced and LBP features are extracted and fed to the IDSS classifier. The algorithm also compares different classifiers including k-NN, ANFIS, SVM, and ANN.

To segment and detect brain tumors from magnetic resonance images a deep learning algorithm is proposed in [13]. The method first pre-processes input images and a hybrid convolutional neural network (CNN) is employed. The algorithm effectively detects test images as healthy or containing tumor. GLCM and DWT features are extracted from the input image and classification of the tumor is done using CNN in [14]. A combination of the ANN and the c-means clustering model is developed for brain tumor detection [15]. GLRLM features are extracted after clustering operation for the classification task.

### III. PROPOSED APPROACH FOR BRAIN TUMOR DETECTION USING MONOGENIC WAVELET PHASE-ENCODED FEATURES

Phase encoded discrimination details in the form of textural features are extracted after monogenic wavelet decomposition for the detection of tumor image. The detailed architecture of the proposed approach is shown in Fig. 1. Magnetic resonance images are first filtered to remove the noise and further enhanced in the pre-processing stage. Phase component of the enhanced MR image is acquired after the monogenic wavelet decomposition. All the phase components are employed for the feature extraction process. CLBP is a popular texture descriptor used in a variety of image processing applications. From each of the phase sub-band, CLBP features are extracted representing abnormalities and variations present in the abnormal tumor image.

To reduce the feature vector dimensionality and to choose the most relevant CLBP descriptors from a pool of large feature set, neighborhood component analysis based feature selection is employed in this work. The optimal

feature set generated by NCA is then fed to support vector machine classifier. The SVM output is a binary decision assigning the label to the test image as healthy or abnormal containing the tumor. The proposed algorithm is validated using two widely used MR image databases: e-health laboratory and Harvard medical-laboratory.

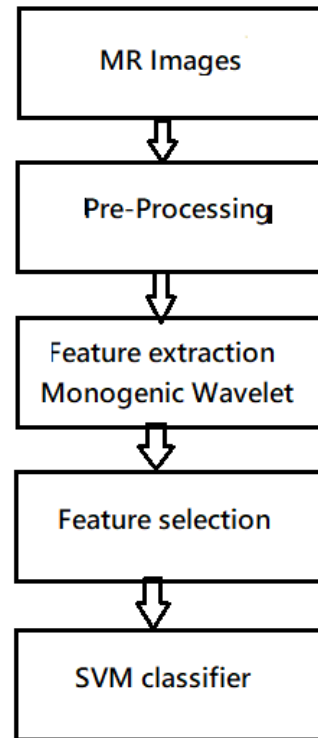


Fig. 1. Monogenic wavelet phase-encoded features based brain tumor image detection architecture.

## IV. FEATURE EXTRACTION AND SELECTION

### A. Pre-processing

MR imaging pre-processing is an influential task to minimize image degradation and in turn to enhance the classification accuracy. In this step, the input image is first resized into  $256 \times 256$  spatial resolution. Resized samples are then converted into grayscale images before the feature extraction process. To remove the noise present in the image, the median filtering is applied. Finally, the filtered image contrast is enhanced using Contrast limited adaptive-histogram equalization (CLAHE).

### B. Monogenic wavelet based phase encoding

Monogenic signal image analysis is based on the analytic signal concept and it generates rotation-invariant amplitude, phase, and orientation components [16]. A two-dimensional image is convolved with a quadrature filter creating the local phase, orientation, and energy components [17]. 2-D Riesz transform is defined as,

$$f_R(i) = \begin{Bmatrix} f_x(i) \\ f_y(i) \end{Bmatrix} = \begin{Bmatrix} k_x * f(i) \\ k_y * f(i) \end{Bmatrix} \quad (1)$$

Where  $f(i)$  is the input signal and  $i = (x, y)$ , filter responses in 2 dimensions are represented as  $k_x$  and  $k_y$ .

Monogenic signal of an image  $f(i)$  is obtained from the Riesz transform as,

$$f_m(i) = f(i), f_x(i), f_y(i) \quad (2)$$

$f(i)$  is the real component of the monogenic signal, and  $f_x(i)$  and  $f_y(i)$  are imagery parts. The input MR image can be decomposed into three components: (1) local phase (2) local amplitude and (3) local orientation, using these real and imaginary parts of the monogenic signal. Various monogenic components are computed as,

- (1) Local amplitude  $A_L = \sqrt{f + f_x^2 + f_y^2}$
- (2) Local phase  $\emptyset = -\text{sign}(f_x) \text{atan2}(\sqrt{f_x^2 + f_y^2}/f)$
- (3) Local orientation  $\theta = \text{atan}(\frac{f_y}{f_x})$

In the above equation,  $A_L$  represents the local energy contents,  $\emptyset$  shows structural details and geometric information is contained in  $\theta$ .

### C. Completed LBP descriptors

In the next stage, CLBP textural features are extracted from all the phase components of the monogenic signal. CLBP is a powerful texture descriptor generated by combining sign, magnitude, and average components locally and used in a variety of image and signal processing applications [18]-[19]. The computation of sign and magnitude component contributes to additional local textural information as compared to the original LBP. The final coded CLBP histogram includes all three components. A detailed description of CLBP computation is described in [20].

### D. Neighborhood component Analysis feature selection:

Feature selection is a principal step in machine learning algorithms to choose relevant features and to remove non-discriminating features. Feature selection approaches are divided into three types: (a) filter methods (b) wrapper methods and (c) hybrid methods [21]. The neighborhood component analysis (NCA) algorithm belongs to the filter method.

NCA is a feature weighting strategy for optimal feature subset selection. It uses objective function maximization criteria by evaluating overage classification accuracy over the training samples. Nearest neighbor classifier optimization generates the final weighting vector from the training data. The final weighting vector corresponding to the feature set is produced without any parametric assumption of the data under consideration and useful in multi-class problems. The objective function in NCA is defined as [22],

$$F = \sum_{i=1}^m O_i - \gamma \sum_{j=1}^r w_j^2 \quad (3)$$

Where  $\gamma$  is the regularization parameter,  $O_i$  is the probability of correct classification of  $i$ th sample,  $w_j$  is the weight vector. As the NCA assigns weight to each of the training samples, threshold  $T$  is set during the experiment to select the most relevant features.

## V. EXPERIMENTAL RESULTS AND DISCUSSIONS

This section presents the simulation results and discussion. Experimental settings and dataset used are

described first and later classification results with and without feature selection approach are presented. 50 healthy and 64 images with tumors are selected from the e-Health laboratory dataset [23] and Harvard medical laboratory [24]. Sample healthy and tumor images are shown in Fig. 2.

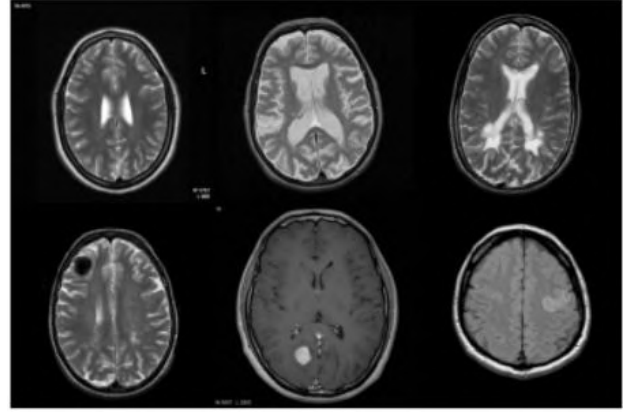


Fig. 2 Sample images from the database containing healthy and tumor samples.

As discussed in section III, selected MR images are pre-processed first. In the median filtering, neighborhood size is set to  $3 \times 3$ . Clip limit is selected as 0.001 while implementing the CLAHE algorithm. A lower clip limit is desirable to achieve better enhancement. Monogenic wavelets can be implemented using a variety of filters. In this work, the *log-Gabor* filter type is employed with a 0.55 shape parameter. Fig. 3 depicts even and odd parts of the frequency domain filters.

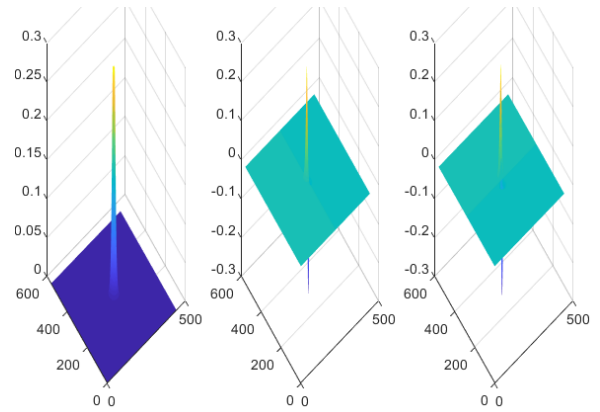


Fig. 3 Even and odd parts of the frequency domain filter.

The neighborhood component analysis approach is a weighting algorithm that assigns weight to an individual feature from the training data. Hence, a threshold-based approach is essential to extract relevant features. In this study, threshold  $T$  is selected experimentally. The support vector machine classifier is implemented using the Lib-SVM package [25]. Radial basis function (RBF) is used as a kernel function in SVM. Best values of cost parameter (C) and gamma  $\gamma$  are obtained using 5-fold cross-validation.

The first experiment involves individual phase-encoded feature evaluation using different sub-bands. Table I shows

sensitivity, specificity, precision, F1-score, and accuracy obtained using SVM classifier with and without NCA feature selection. RBF kernel function is used during SVM implementation. The first and third phase-encoded descriptors contribute higher as compared to the second descriptor. It is important to note that, in the first and second component the accuracy remained the same even after NCA feature selection. However, in the first case the feature vector dimension was reduced from 118 to 30 and in the second case to 72. So, NCA is a powerful feature selection algorithm that reduces the dimensionality of the feature set.

TABLE I  
DIFFERENT PARAMETER EVALUATION USING INDIVIDUAL PHASE-ENCODED COMPONENT WITH AND WITHOUT FEATURE SELECTION.

Features	NCA	Sensitivity	Specificity	Precision	F1	Accuracy
Monogenic wavelet phase component 1	Yes	100	86.67	86.67	0.9267	93.33
	No	100	86.67	86.67	0.9267	93.33
Monogenic wavelet phase component 2	Yes	69.23	93.33	90	0.7826	92.82
	No	69.23	93.33	90	0.7826	92.82
Monogenic wavelet phase component 3	Yes	92.31	93.33	92.31	0.9231	92.82
	No	92.31	100	100	0.96	96.75

The second experiment involves the fusion of all the three phase components and evaluation of the parameters. Table II depicts various performance evaluation parameters obtained using RBF-SVM with and without feature selection technique. As it can be seen from table II that the highest accuracy is attained by applying neighbourhood component analysis feature selection. After NCA, the final feature vector length recorded was 54. Hence, the phase component of the monogenic wavelet efficiently extracts the structural information from the input magnetic resonance images useful for the classification task. It is interesting to note here that, this experiment uses only monogenic phase-encoded features without the inclusion of energy and orientation components.

TABLE II  
DIFFERENT PARAMETER EVALUATION USING THE FUSION OF PHASE-ENCODED COMPONENTS WITH AND WITHOUT FEATURE SELECTION.

	NCA	Sensitivity	Specificity	Precision	F1	Accuracy
Fusion of monogenic wavelet phase component	Yes	100	100	100	1	100
	No	92.86	100	100	0.963	96.43

As discussed in section IV, the neighborhood component analysis approach is employed for feature selection. NCA is a feature weighting technique that assigns weight to an individual feature from the training data. The weighted features are ranked according to the

individual weight in this study. Different threshold  $T$  is set and the accuracy rate is computed. Figure 4 illustrates different NCA thresholds  $T_1 T_2 \dots T_6$  and its corresponding classification accuracy. It is evident from figure 4 that the classification rate is significantly enhanced after the threshold value  $T_5$ .

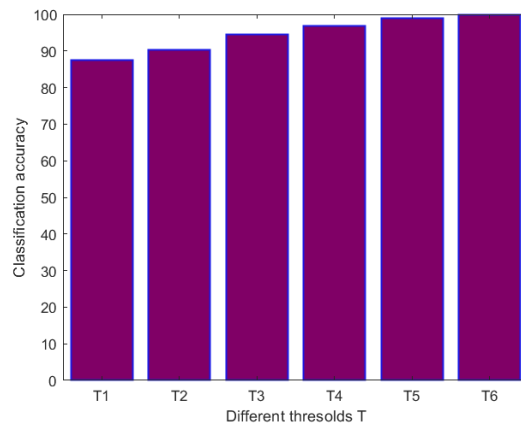


Fig. 4 Effect of feature selection using different threshold values on the classification accuracy.

The proposed monogenic wavelet phase-encoded MR brain tumor image detection algorithm is compared to other existing algorithms. Table III shows the comparison of various algorithms with the proposed monogenic wavelet phased encoding approach. It is clear from table III that, phase components accurately extracts abnormality details from the input image useful for the classification task. It is also interesting to note that transform domain feature extraction techniques perform better as compared to spatial domain features.

TABLE III  
COMPARISON OF THE PROPOSED APPROACH WITH OTHER EXISTING ALGORITHMS.

Method	Features	Classifier	Accuracy (%)
[3]	Textural features from wavelet, curvelet and shearlet transform	PSO-SVM	97.38
[4]	LBP and Gabor wavelet function	KNN	98
[6]	Local Ternary Pattern (LTPs) and Local Quinary Patterns (LQPs)	SVM & KNN	97.5
[7]	k-means clustering	ANN	94.07
[8]	Geometric and four texture features	SVM	99.99
[9]	Energy and variance features from DWT sub-bands	ANN	99.7
Proposed	Monogenic wavelet phased encoded features	SVM	100

## VI. CONCLUSION

The efficient extraction of structural information by the monogenic wavelet phase components is presented for brain tumor image detection. The proposed algorithm detects input test MR image as healthy or containing tumor with high accuracy evaluated using two popular magnetic resonance imaging datasets. Additionally, neighborhood component analysis reduces the feature vector

dimensionality with affecting the classification rate considerably. The method performs better as compared to other similar brain tumor detection algorithms. Future analysis includes effect of the monogenic wavelet energy and orientation components on the detection rate.

#### REFERENCES

- [1] Indian Brain tumor statistics. [https://www.nhp.gov.in/world-brain-tumour-day2019\\_pg](https://www.nhp.gov.in/world-brain-tumour-day2019_pg) (Accessed on 17 September 2020)
- [2] S. Iqbal, S. Khan, M. Saba, A. Rehman, "Computer-assisted brain tumor type discrimination using magnetic resonance imaging features", *Biomedical Engineering Letters*, vol.8, no.1, pp. 5-28, February 2018.
- [3] A. Gudigar, U. Raghavendra, T. San, E. Ciaccio, U. Acharya, "Application of multiresolution analysis for automated detection of brain abnormality using MR images: A comparative study", *Future Generation Computer Systems*, vol.90, pp. 359-367, January 2019.
- [4] J. Amin, M. Sharif, M. Raza, T. Saba, M. Anjum, "Brain tumor detection using statistical and machine learning method", *Computer Methods and Programs in Biomedicine*, vol. 177, pp. 69-79, August 2019.
- [5] C. Han, L. Rundo, R. Araki, Y. Furukawa, G. Mauri, H. Nakayama H. Hayashi, "Infinite Brain MR Images: PGGAN-Based Data Augmentation for Tumor Detection", *Neural Approaches to Dynamics of Signal Exchanges*, pp. 291-303, 2019.
- [6] M. Zafar, S. Adnan, J. Rashid, W. Admad, J. Ikram, "Brain Tumor Detection and Classification Using Geometrical Shapes as Texture Descriptors", *Technical Journal, University of Engineering and Technology (UET) Taxila*, vol. 24, no. 1, pp. 83-89, March 2019.
- [7] N. Arunkumar, M. Mohammed, M. Ghani, D. Ibrahim, E. Abdulhay, G. Ramirez-Gonzalez, V. Albuquerque, "K-Means clustering and neural network for object detecting and identifying abnormality of brain tumor", *Soft Computing*, vol. 23, pp. 9083-9096, October 2019.
- [8] M. Sharif, U. Tanvir, E. Munir, M. Khan, M. Yasmin, "Brain tumor segmentation and classification by improved binomial thresholding and multi-features selection", *Journal of Ambient Intelligence and Humanized Computing*, pp. 1-20, October 2018.
- [9] M. Nazir, M. A. Khan, T. Saba, A. Rehman, "Brain Tumor Detection from MRI images using Multi-level Wavelets," *2019 International Conference on Computer and Information Sciences (ICCIS)*, Sakaka, Saudi Arabia, pp. 1-5, 2019.
- [10] J. Amin, M. Sharif, M. Yasmin, T. Saba, M. Raza, "Use of machine intelligence to conduct analysis of human brain data for detection of abnormalities in its cognitive functions", *Multimedia Tools and Applications*, pp. 1-19, February 2019.
- [11] T. Pandiselvi, R. Maheswaran, "Efficient Framework for Identifying, Locating, Detecting and Classifying MRI Brain Tumor in MRI Images", *Journal of Medical Systems*, vol. 43, no. 7, pp. 1-14, July 2019.
- [12] S. Polepaka, S. Rao, C. Mohan, "IDSS-based Two stage classification of brain tumor using SVM", *Health and Technology*, pp. 1-10, January 2019.
- [13] S. Sajid, S. Hussain, A. Sarwar, "Brain Tumor Detection and Segmentation in MR Images Using Deep Learning", *Arabian Journal for Science and Engineering*, vol.44, no.11, pp. 9249-9261, November 2019.
- [14] K. Bhargavi, J. Mani, "Early Detection of Brain Tumor and Classification of MRI Images Using Convolution Neural Networks", *Innovations in Computer Science and Engineering. Lecture Notes in Networks and Systems*, vol 74. Springer, pp. 427-436, June 2019.
- [15] Parveen, A. Singh, "Detection of Brain Tumor in MRI Images, Using Fuzzy C-Means Segmented Images and Artificial Neural Network", *Proceedings of the International Conference on Recent Cognizance in Wireless Communication & Image Processing*, pp. 123-131, April 2016.
- [16] M. Felsberg, G. Sommer, "The monogenic signal", *IEEE Transactions on Signal Processing*, vol. 49, no. 12, pp. 3136-3144, 2001.
- [17] P. Birajadar, M. Haria P. Kulkarni, S. Gupta, P. Joshi, B. Singh, V. Gadre, "Towards smartphone-based touchless fingerprint recognition", *Sādhanā*, vol.41, no.161, pp. 1-15, 2019.
- [18] M. Muqet, R. Holambe, "A collaborative representation face classification on separable adaptive directional wavelet transform based completed local binary pattern features", *Engineering Science and Technology, an International Journal*, vol. 21, pp. 611-624, 2018.
- [19] A. Chowdhury, V. Borkar, G. Birajdar. "Indian language identification using time-frequency image textural descriptors and GWO-based feature selection", *Journal of Experimental & Theoretical Artificial Intelligence*, vo.32, no.1, pp. 111-132, 2020.
- [20] Z. Guo, L. Zhang, D. Zhang, "A Completed Modeling of Local Binary Pattern Operator for Texture Classification", *IEEE Transactions on Image Processing*, vol. 9, no. 16, pp. 1657-1663, 2010.
- [21] G Chandrashekar, F. Sahin, "A survey on feature selection methods", *Computers & Electrical Engineering*, vol.40, no. 1, pp. 16-28, 2014.
- [22] W. Yang, K. Wang, W. Zuo. "Neighborhood Component Feature Selection for High-Dimensional Data", *Journal of Computers*, vol. 7, no. 1, pp. 161-168, January, 2012.
- [23] eHealth Laboratory database: (accessed December 28, 2019), <http://www.medinfo.cs.ucy.ac.cy/index.php/downloads/datasets>
- [24] Harvard Medical School Database: (accessed December 28, 2019), <http://www.med.harvard.edu/aanlib>
- [25] C. Chang, CJ Lin, LIBSVM: A library for support vector machines. *ACM Transactions on Intelligent Systems and Technology*, vol. 2, no. 27, pp. 1-27, 2011.

## Brain Tumor segmentation with Anti-Aliasing Impact filtration using Modified Finite Impulse Response Linear filter

<b>Smita Kakade</b> Research Scholar Computer Department JJTU, Jhunjhunu Rajasthan 333001	<b>Dr.Vinod M. Vaze,</b> Rtd. MCA Coordinator., MU Professor Computer Sc. JJTU, Jhunjhunu Rajasthan 333001	<b>Dr.Pankaj Agarkar</b> D.Y.Patil COE Lohagaon Pune 411032 Maharashtra	<b>Deepali Hirolikar</b> Research Scholar Computer Department JJTU, Jhunjhunu Rajasthan 333001
--	--	---	---

### Abstract:

The field of medical imaging advances so rapidly that all of those working in it, scientists, engineers, physicians, educators and others, need to frequently update their knowledge in order to stay abreast of developments. While computer engineering play a crucial role in this, more extensive, integrative research of image processing that connect fundamental principles and advances in algorithms and techniques to practical applications are essential. We focused on development of new medical imaging techniques which can serve the medical society.

Treatment protocols for malignant tumors generally call for surgical removal followed by tumor-bed irradiation. Irradiation ideally affects the tumor volume while limiting damage to surrounding normal tissues, this required accurate determination of 3-D treatment volumes.

Accurate tumor segmentation provides doctors with a basis for surgical planning. Moreover, brain tumor segmentation need to extract different tumor tissues from normal tissues which is a big challenge because tumor structures vary considerably across patients in terms of size, extension, and localization.

We need methodology to reconstruct image to refine boundary of objects present image. Proposed methodology shows clearvisibility of tumor growth along with anti-aliasing element which eliminates blood, plasma, fluid impurities and focuses over brain tumor affected area and assists the surgeon during actual surgery.

### 1. Background:

We will consider a base as a super sampling anti-aliasing (SSAA), also called full-scene anti-aliasing (FSAA), is used to avoid aliasing on full-screen images. Due to its tremendous computational cost and the advent of multi-sample anti-aliasing (MSAA) support on GPUs, it is no longer widely used in real time applications. MSAA provides somewhat lower graphic quality, but also tremendous savings in computational power.

The resulting image of SSAA may seem softer, and should also appear more

realistic. However, while useful for photo-like images, a simple anti-aliasing approach may actually worsen the appearance of some types of line art or diagrams, especially where most lines are horizontal or vertical. In these cases, a prior grid-fitting step may be useful.

In general, super-sampling is a technique of collecting data points at a greater resolution (usually by a power of two) than the final data resolution. These data points are then combined (down-sampled) to the desired resolution, often just by a simple average. The combined

data points have less visible aliasing artefacts.

Automated classification is encouraged by the need for high accuracy in dealing with a human life. Detection of brain tumor is a challenging problem due to the high diversity in tumor appearance and ambiguous tumor boundaries. MRI images are chosen for the detection of brain tumors as they are used in the determination of soft tissues.

The most precious field in digital image processing is diagnosing the internal activities of human body. Brain is one of the critical part in human body. In the current era cancer is a challenging in medical field. Identification of tumor in brain is very difficult. Segmentation is a kind of method in digital image processing used to divide the image into number of parts with specific regions.

Researches on classification for brain tumor from MRI image had been done extensively, yet there is still room for improvement. Anti-aliasing methods mentioned above will not work for medical imaging used for surgery. At first need to select features for pixel sampling. Many approaches had been focused on image segmentation and classification algorithm, yet little number of researches done on feature selection. Domain knowledge of medical science can be gained from medical practitioners to define characteristics of tissue of tumor and normal tissues. Images can be taken which don't have copyright.

In medical field, image fusion is a significant role analyzed the brain tumor which can able to get exact location and boundary of cancerous or noncancerous region. It is the method in which many images are integrated to a similar view into single fused image. This image is to decrease the uncertain and minimize the redundancy while extracting all the useful

information through the input source images. The image fusion system is the combination of multi-images with relative data into single image. This method can be used to notice the brain tumor by combining T1 and T2 MRI slice images. Tumor segmentation is done using the level set segmentation method. Then the feature extraction is done with the complete local binary pattern approach and pyramid HOG approach. ART classifier can also used to classify the brain tumor to malignant or benign. Accurate and reliable brain tumor segmentation is a critical component in cancer diagnosis, treatment planning, and treatment outcome evaluation.

A variety of approaches exist for brain extraction from 3D medical images, but they are frequently only designed to perform brain extraction from images without strong pathologies. Extracting the brain from images exhibiting strong pathologies, for example, the presence of a brain tumor or of a traumatic brain injury (TBI) is challenging. In such cases, tissue appearance may substantially deviate from normal tissue appearance and hence violates algorithmic assumptions for standard approaches to brain extraction consequently

## 2. Motivation:

Computer processing and analysis of medical images covers a broad number of potential topic areas, including image acquisition, image formation/reconstruction, image enhancement, image compression and storage, image analysis, and image-based visualization. Furthermore, we need the research efforts related to these methodologies are the key elements of solutions to more systems-oriented problems. Such problems include image-guided surgery/intervention, atlas-based description of entire anatomical regions, deformation analysis based on biomechanical and other models, and

visualization of anatomical and physiological processes.

Objectives of this research work are to image enhancement and segmentation for cancerous and normal medical image data, anti-aliasing framework will be designed and implemented.

### 3. Methodology:

Segmentation task is different from classification task because it requires predicting a class for each pixel of the input image, instead of only one class for the whole input. Fully Convolutional Networks (FCNs) owe their name to their architecture, which is built only from locally connected layers, such as convolution, pooling and up sampling. Note that no dense layer is used in this kind of architecture. This reduces the number of parameters and computation time.

The size of the images varies. We use data augmentation for training, as specified in the default arguments in the code given below. The data augmentation is necessary for training with batch size greater in order to have same image size with a random cropping. For validation and test sets with exact results, full dataset training is required for performance evaluation which takes many days to run and overshoots memory problems.

The proposed research intended for classification of different levels of tumor as T1, T2, T1ce and Fluid Attenuated Inversion Recovery (FLAIR). At the time of MRI accumulation, even though may differ by system to system, about 150 slices of 2D images are actually generated to symbolize the 3D brain volume level. The moment when the slices of the needed typical techniques are put together for analysis of the data becomes somewhat complex. T1 images are actually utilized for differentiating healthier cells, while T2 images are actually utilized to represent

the edema area which in turn generates idealistic indication around the image. In T1ce graphics, the tumor boundary can simply be recognized through white-colour signal from the accrued distinction element inside the effective cell area of the tumor cells. As necrotic microscopic cells usually do not have interaction with the entire comparison agent, these may be noticed by extreme component of the tumor foremost developing it feasible to conveniently segment all of them by the productive cell areas within the comparable pattern. In FLAIR images, indication of water compounds are covered up which usually assists in differentiating edema area through the Cerebrospinal Fluid (CSF).

The proposed research methodology is a simulation development. Convolution Neural Networks (CNN) is amongst the alternatives of neural systems utilized intensely in the discipline of Computer system Vision. It was introduced their identity by the variation of obscured layers that is composed of the obscured layers of the CNN ordinarily comprise of convolution and pooling layers. Right here it basically suggests that rather of applying the typical initialization features described earlier, convolution and as well, pooling features are actually employed as acceleration operates.

Convolution works upon pair of images in case of 2D image where 1 considered as the "input" graphic and so the rest as a "filters" for the input image, generating a result graphic so convolution requires pair of images as input and so delivers a final as end result. Pooling is usually a group centred discretization procedure. The goal is always to reducing-group an input manifestation minimizing its proportions and enabling for presumptions to become relating to features comprised within the sub-areas. Therefore since one can easily observe Convolution Neural Networking i.e. CNN is fundamentally a deep neural networking which generally is composed of covered

layers keeping convolution and so pooling capabilities in companion to the initial function for producing nonlinear output.

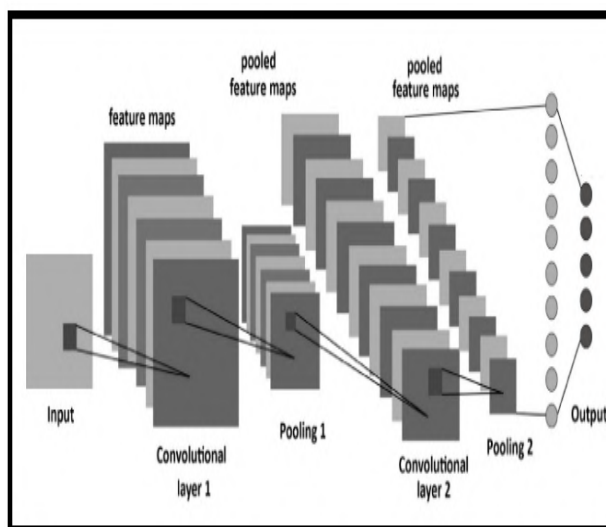


Figure 1–Block diagram of deep learning layers

#### 4 Proposed Methodology

We shared our experimental results with team of ten medical professionals to validate present research, two radiologists, five surgeons and three anaesthetists studied and validated the usability of present research. Most of these team members have been in specialty practice and carried out processes at the hospital in Maharashtra State region in India.

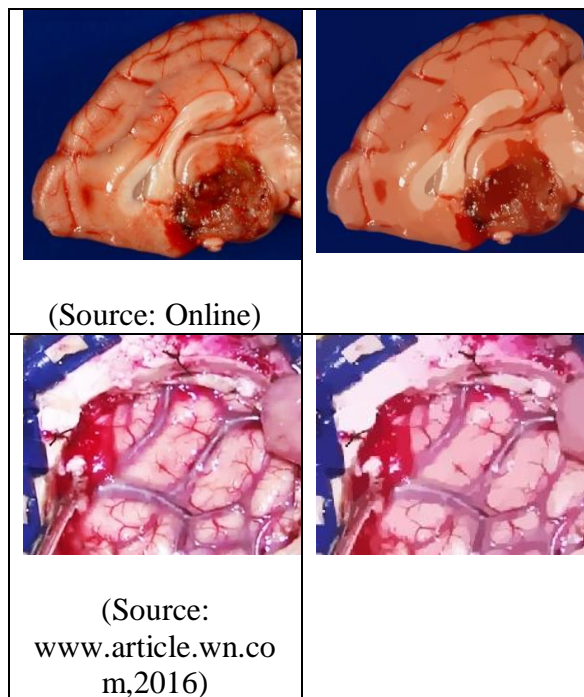
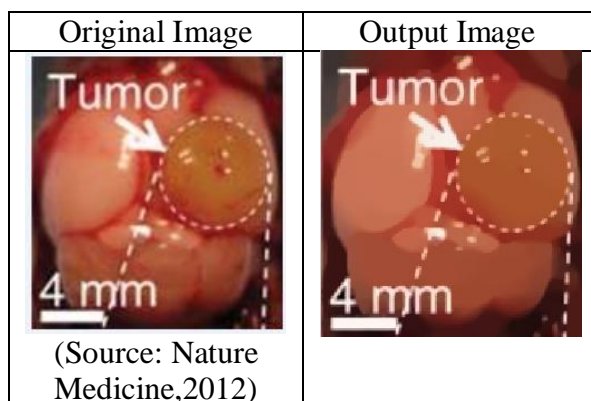


Figure -2: Brain tumor surgical Image testing with DTR Adapter Module

The team tested real-time images and processed it with DTR with our assistance. The results are positive and can be recommended for medical imaging during surgical image captures. As of now, the output shows clear visibility of tumor growth, and surgeons can remove the tumor but, it is important to make sure that tumor is removed perfectly.

Considering that the studies are produced in a very organized structure, we used images captured during neuroendoscopy. The anti-aliasing element eliminates blood, plasma, fluid impurities and focuses over brain tumor affected area and assists the surgeon during actual surgery. Further, this defogged image output can be treated with “tumor routing” algorithm. We also analyzed offline method; the benefit of using defogged MR image instead of original MR image is that defogged image gives accurate positioning of tumor dimensions as shown using graphs in figure above.

The graphical representation shows the vertical and horizontal position of the tumor. With knowledge of graphical representation, the surgeon can be able to visualize live image during surgery. Also in the case of MRI, if further image streaming is developed, the surgeon may check how much tumor is removed, and by using graph location he/she can identify which part of the tumor needs to remove. When both points on each graph overlaps it means tumor removal is successful by tumor routing i.e. the process of step by step tumor removal.

### Algorithm 1: Anti-Aliasing

1. Input MRI image which was captured before or after surgery to know the vertical state of tumor growth. We can use MRI image too, but the aim of the present module is to show the overall volume of the skeleton to identify the volumetric impact of the tumor.
2. Compute main pixel window (horizontal plane) for MRI image
3. Compute main pixel window (vertical plane) for MRI image.
4. Store horizontal and vertical window boundary pixels location in array-1 and array-2
5. Calculate high-intensity pixel for vertical count
6. Route through vertical pixels and Join high-intensity points
7. Stores it as a vertical shift tumor boundary location
8. Analyze 3D view for vertical shifting points and mark it.
9. If there are zero vertical shifts for low-intensity pixels, then consider end point of vertical shift.

10. Identify and compare highest intensity pixels in each tumor slice and connect initial pixel and final pixel.

This algorithm is intended for visual analysis for surgeons and can be used for pre and post surgical activities. The Tumor Removal Analyzer algorithm provides a 3D view which provides more clear visibility for tumor shift. Following figure-5 provides step by step analysis for brain tumor.

### 5. Results:

The proposed work considered an applied mathematics research. Proposed application oriented mathematical modelling flow is shown in figure below. Mathematical model is used to interact with each image pixel using set rules which can be used for the identification of tumor images pixels. The set rule will work on gray pixels and white pixels.

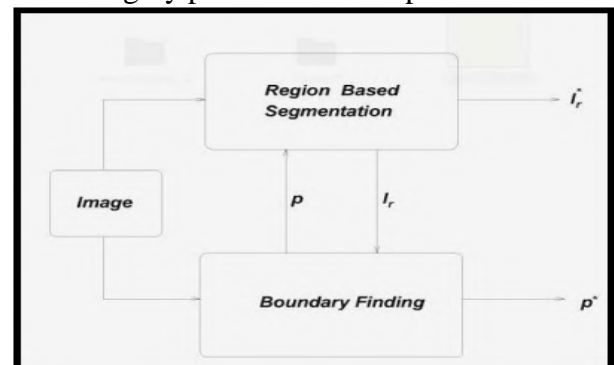


Figure 3- Flow Diagram for game theoretic image segmentation (Source: Online)

We developed modified Finite Impulse Response Linear filters for brain tumorgrey pixel identification. We considered FIR mathematical model as a reference model and this is further developed for MRI image pixel filtering. The game theory model will be applied for strategic pixel count calculation. We considered region growing problem for evaluation of proposed brain tumor image processing application as shown in figure below.

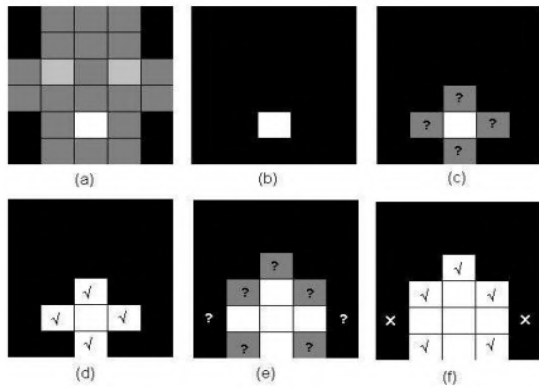


Figure 4- Region of Interest Pixel Clustering

The Modified Finite Impulse Response Linear filter (MFIR) further segregates the tumor tissue pixels and normal brain tissue pixels. In reference model only border of tumor is identified whereas in proposed mathematical model we can separately calculate the healthy tissues and tumor tissues accurately. Thus for MRI brain tumor image input proposed model gives more accuracy than existing model. We used images upload to Hadoop Server which is used as a medical image storage cluster. The mathematical model is converted to python for testing purpose. The following figure 3 shows the successful porting of mathematical model which further converted to algorithm by software professional for testing.

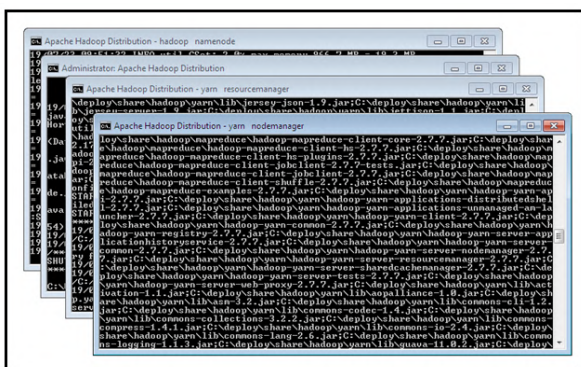


Figure 5 –Hadoop image storage cluster

The proposed game theory strategy for MFIR proved the better in terms of accuracy and feature extractions. For proposed model testing we used BRATS 2018 dataset images for 81 patients.

Table-1: Proposed Mathematical Model Performance Analysis

Model	Pixel Accuracy	Feature Extraction	Application level usability
MFIR (Proposed Model)	97%	Normal brain tissues, Tumor tissue	Yes
FIR	94%	Tumor tissue	Yes

Thus the MFIR and FIR outputs for same image are shown in figure 4.5 below:



(a)MFIR

(b)FIR

The MFIR shows the middle healthy tissues whereas FIR shows the middle bunch of pixels as a whole tumor. So, during surgery, whole part will be considered as a removal area in case of FIR but with MFIR, many tissues can be saved due to clear visibility of infected/tumor tissues.

### Conclusion

Machine Learning (ML) and Artificial Intelligence (AI) have progressed rapidly in recent years. Techniques of ML and AI have played important role in medical field like medical image processing, computer-aided diagnosis, image interpretation, image fusion, image registration, image segmentation, image-guided therapy, image retrieval and analysis. Techniques of ML extract information from the images and represents information effectively and efficiently. The ML and AI facilitate and

assist doctors that they can diagnose and predict accurate and faster the risk of diseases and prevent them in time. These techniques enhance the abilities of doctors and researchers to understand that how to analyse the generic variations which will lead to disease.

## References

- [1] AbbasiSolmaz and FarshadTajeripour. "Detection of brain tumor in 3D MRI images using local binary patterns and histogram orientation gradient." *Neurocomputing* (2017) ,Vol. 219, Pp. 526-53, DOI: [10.1016/j.neucom.2016.09.051](https://doi.org/10.1016/j.neucom.2016.09.051)
- [2] Abdel-MaksoudEman, Mohammed Elmogy and Rashid Al-Awadi. "Brain tumor segmentation based on a hybrid clustering technique." *Egyptian Informatics Journal*(2015), Vol.16.1,Pp. 71-81, DOI: 10.1016/j.eij.2015.01.003
- [3] Akram M. Usman and AnamUsman. "Computer aided system for brain tumor detection and segmentation." *International Conference on Computer Networks and IT. IEEE,2011, ISSN: 2223-6317, DOI :10.1109/ICCNIT.2011.6020885*
- [4] AslamAsra, Ekram Khan and MM Sufyan Beg. "Improved edge detection algorithm for brain tumor segmentation." *Procedia Computer Science* Vol.58(2015), Pp.430-437, DOI:10.1016/j.procs.2015.08.057
- [5] Bjoern H. Menze, AndrasJakab and Stefan Bauer "The multimodal brain tumor image segmentation benchmark (BRATS)." *IEEE transactions on medical imaging* Vol. 34.10 (2014), Pp.1993-2024, ISSN: 1558-254X, DOI: [10.1109/TMI.2014.2377694](https://doi.org/10.1109/TMI.2014.2377694)
- [6] BaraiyaNeha and HardikModi. "Comparative study of different methods for brain tumor extraction from MRI images using image processing." *Indian Journal of Science and Technology* Vol. 9.4 (2016), DOI:10.17485/ijst/2016/v9i4/85624, ISSN : 0974-5645.
- [7] Bauer Stefan, Wiest R and Nolte LP "A survey of MRI-based medical image analysis for brain tumor studies." *Physics in Medicine & Biology* Vol. 58.13 (2013), Pp. 97-129, DOI: 10.1088/0031-9155/58/13/R97
- [8] Chen Shengcong, Changxing Ding and MinfengLiu."Dual-force convolutional neural networks for accurate brain tumor segmentation." *Pattern Recognition*, Vol. 88 (2019), Pp. 90-100, DOI: 10.1016/j.patcog.2018.11.009
- [9] Chen Shengcong, Changxing Ding and MinfengLiu."Dual-force convolutional neural networks for accurate brain tumor segmentation." *Pattern Recognition*, Vol. 88 (2019), Pp. 90-100, DOI: 10.1016/j.patcog.2018.11.009



## A Stereolithography System for 3D Low Cost Components

Baban K. Suryatal<sup>1,2\*</sup>, Sunil S. Sarawade<sup>3</sup>, Suhas P. Deshmukh<sup>4</sup>

<sup>1</sup> Mechanical Engineering Department, Sinhgad College of Engineering, Vadgaon Bk., Savitribai Phule Pune University, Pune, Maharashtra 411041, India

<sup>2</sup> Mechanical Engineering Department, PDEA's College of Engineering, Manjari Bk., Pune, Maharashtra 412307, India

<sup>3</sup> Mechanical Engineering Department, M.E.S. College of Engineering, Pune, Maharashtra 411001, India

<sup>4</sup> Mechanical Engineering Department, Government Engineering College, Karad, Maharashtra 415124, India

Corresponding Author Email: [bksuryatal@gmail.com](mailto:bksuryatal@gmail.com)

<https://doi.org/10.18280/jesa.530312>

### ABSTRACT

**Received:** 9 February 2020

**Accepted:** 23 April 2020

#### Keywords:

*photo-polymer, stereolithography, rapid prototyping, ultra-violet light*

The stereolithography (SL) process is one of the rapid prototyping technics and it is also known as additive layered manufacturing method. It is a chipless manufacturing method and the object is built layer by layer. A low cost stereolithography apparatus (SLA) is developed to produce highly precise, three-dimensional (3D) structures from broad selection of functional materials, especially photopolymer resin. The present SL systems available in the market are very expensive. The developed low cost SLA will be affordable to medium scale industries as well as customers. The developed SLA utilizes focused light beam of wavelength range of 300 nm – 700 nm from the DLP projector and passes through the objective lens over the surface of a photo-curable resin, which undergoes photopolymerization and forms solid structures. The photopolymer used in this experimentation is polyethylene glycol di-acrylate and photo-initiator is Irgacure 784. The experiments are performed on objects with hexagonal cross-section and pyramid geometries and 0.1 mm curing depth along Z – axis. The trials are performed with different exposure and settling period. The 3D objects are successfully fabricated with high build speed and low cost. The pyramid object with maximum 120 numbers of layers with 12 mm dimension along Z-axis is built in 11.0 minutes. It is found that the optimum exposure time to cure a layer is two seconds. The maximum exposure area obtained in X-Y plane is 55 mm x 45 mm. The percentage dimensional error of the build objects is decreased as the curing time is reduced and the error is minimum for the two seconds curing period per layer. The obtained resolution of the build objects in X-Y plane is 23 microns and Z-stage resolution is 0.1 mm.

## 1. INTRODUCTION

There are a number of processes that can realize three-dimensional (3D) shapes such as those stored in the memory of a computer. An example is the use of holographic techniques [1], but these require many complex calculations to obtain the hologram and there is insufficient accuracy and clarity. A manual or a conventional mechanical process can also make a physical model, but such models require long fabricating times, high cost and excessive labour. To solve these kinds of problems, a new group of techniques called additive manufacturing (AM) technologies have been developed by a number of researchers group [2-5]. AM is a collection of processes in which physical objects are quickly created directly from computer generated models. The basic concept of rapid prototyping is where 3D structures are formed by laminating thin layers according to two-dimensional (2D) slice data, obtained from a 3D model created on a CAD/CAM system [2-5]. Stereolithography (SL) is one of the most popular AM process. It usually involves the curing or solidification of a liquid photosensitive polymer by focusing a light beam or laser beam of specific wavelength on the surface with liquid photopolymeric resin. The focused light beam supplies energy that induces a chemical reaction, bonding

large number of small molecules and forming a highly cross-linked polymer [6]. Now a day, rapid prototypes of the different objects are required before their actual manufacturing because one can improve the design at the early stage of product development. The rapid prototyping or 3D printing field is very fast developing and this technology can applicable to all the fields i.e. engineering as well as non-engineering. The objective of this research work is to develop a low cost stereolithography apparatus (SLA) to produce highly precise, three-dimensional (3D) structures from broad selection of functional materials, especially photopolymer resin. The present SL systems available in the market are very expensive. The overall cost of the newly developed SLA is very low as compared to cost of SLA available in the market. The cost of photo-curable resin used is also low as compared to other available resins. Therefore, the developed low cost SLA will be affordable to medium scale industries and customers as the overall build cost of the objects is minimum.

A large number of researcher's groups have developed the SL systems out of which some of them are briefed in the following literature review.

Fujimasa [7] has been described the concepts of microplanes, microrobots, microcars and microsubmarines and MEMS which are systems that combine computers with

tiny mechanical devices such as sensors, valves, gears, mirrors, and actuators embedded in semiconductor chips. Ventura et al. [8] developed a direct photo shaping process for the fabrication of functional ceramic components layer by layer and each layer is photo image or a digital light processing (DLP) projection system. Bertsch et al. [9] developed a micro stereolithography apparatus employing a pattern generator in which a UV laser and dynamic LCD pattern generator were used to generate the cross section of a 3D structure. While the substrate did not move in the x–y direction in the liquid photopolymer, an LCD pattern generation system was necessary and the resulting diffraction had to be considered. Maruo et al. [10] developed two-photon polymerization (TPP) which utilizes focused lasers to precisely polymerize small volumes resin and the volume is only polymerized if it is excited by two different photons within a very short time period. TPP is much slower than SL, but has successfully created components with 100 nm features. TPP is limited to polymers because it requires a clear resin to function; suspended particles would scatter the laser beams. Young et al. [11] have described a novel device for producing 3D objects that has been developed using an LCD as a programmable, dynamic mask and visible light to initiate photopolymerization. Ikuta et al. [12] introduced micro stereolithography technology and proposed a means of applying micro stereolithography in mass-production using an optical fiber array so that multiple microstructures could be fabricated in a single process. Monneret et al. [13] presented a new process of microstereolithography to manufacture freeform solid 3D micro-components with outer dimensions in the millimeter size range. Sun et al. [14] performed Monte Carlo simulations and experimental studies to understand the detailed microscale optical scattering, chemical reaction (polymerization), and their influence on critical fabrication parameters. It was found that due to the scattering, the fabricated line is wider in width and smaller in depth compared with polymeric fabrication at the same condition. The doping technique substantially reduced the light scattering, which in turn enhanced the fabrication precision and control. The experimental values of curing depth and radius agreed reasonably well with the theoretical modeling. Bertsch et al. [15] described new polymer/composite photosensitive resins that can be used in the microstereolithography process for manufacturing complex 3D components. Huang et al. [16] analyzed the shrinkage deformation of the mask type stereolithography process. Lee et al. [17] developed a micro stereolithography apparatus using a UV laser and a complex optical system. Jiang et al. [18] developed a Masked Photopolymerization Rapid Prototyping (MPRP) system using LCD panel as dynamic mask with an upper exposure skill. Dongkeon et al. [19] developed a liquid crystal display (LCD) based micro stereolithography process in order to fabricate microparts with superior mechanical properties (for e.g., micro gears) and investigates the fabrication process of micro bevel gears using photosensitive resins reinforced with ceramic nanoparticles. Deshmukh et al. [20] proposes and develops an offaxis lens scanning technique for MSL and carries out optical analysis to compare its performance with the existing techniques mentioned above. The comparison clearly demonstrates improved performance with the proposed offaxis lens scanning technique. Limaye [21] presented a more sophisticated process planning method to build a part with constraints on dimensions, surface finish and build time and formulated an adaptive slicing algorithm that slices a CAD

model so as to obtain the required trade-off between build time and surface finish of up facing surfaces of the part. Hadipoesito et al. [22] developed DMD based UV micro – stereolithography system for fabricating 2D and 3D micro – parts. With the help of characterization experiments it was observed that the developed the DMD based imaging system irradiates an entire photopolymer layer at once, providing reasonable curing speed and good resolution at a low cost. Micro parts were also fabricated in nanocomposites, which were obtained by ultrasonic mixing of the transparent photopolymer and nano-sized ceramic particles. The micro models fabricated by this process could be used for micro scale investment casting, tooling, devices, and medical applications. In this method process optimization is needed to improve the quality of fabricated micro – parts. Singhal et al. [23] has presented a statistical surface roughness model for SLS prototypes as a key to slice the tessellated CAD model adaptively. The adaptive slicing system is implemented as Graphic User Interface in MATLAB-7.

Choi et al. [24] developed a more economical and simpler micro-stereolithography technology using a UV lamp as a light source and optical fiber as the light delivery system and photopolymer solidification experiments were conducted to examine the characteristics of the developed micro-stereolithography apparatus. Zhao et al. [25] developed a thick film mask projection stereolithography to fabricate films on fixed flat substrate and develop a column cure model in which a CAD model of part is discretized into vertical columns instead of being sliced into horizontal layers, and all columns get cured simultaneously till the desired heights. Vatani et al. [26] optimized the exiting slicing algorithms for reducing the size of the files and memory usage of computers to process them. In spite of type and extent of the errors in STL files, the tail-to-head searching method and analysis of the nearest distance between tails and heads techniques were used. As a result STL models sliced rapidly, and fully closed contours produced effectively and errorless. Deshmukh et al. [27] carried out analysis and experimental verification of optomechanical scanning systems for microstereolithography. Choi et al. [28] developed MSL system for tissue engineering using a Digital Micromirror Device (DMD) for dynamic pattern generation and an ultraviolet (UV) lamp filtered at 365 nm for crosslinking the photoreactive polymer solution. Gandhi et al. [29] proposes and analyses a 2D optomechanical-focused laser spot scanning system for microstereolithography which allows uniform intensity focused spot scanning with high speed and high resolution over a large range of scan. Higher speed and high resolution at the same time are achieved by use of two serial double parallelogram flexural mechanisms with mechatronics developed around them. Itoga et al. [30] developed maskless photolithography device by modifying Liquid Crystal Display (LCD) projector optics from magnified to reduced projection. The developed device produces a practical centimeter scale micro-pattern by dividing a large mask pattern and divisionally exposing it synchronized with an auto – XY stage, applying it to cell micro-pattern and microfluidic device production. But they arise problems in jagged pattern boundaries due to the liquid crystal panel structure and collapse pattern of the boundary divided on divisional exposure using the auto – XY stage. Zhou et al. [31] presented a novel AM process based on the mask video projection. For each layer, a set of mask images instead of a single image are planned based on the principle of optimized pixel blending. Experimental results show that the mask video

projection process can significantly improve the accuracy and resolution of built components. The disadvantage of this method is that it will require an additional linear stage with good accuracy and moving speed. In addition, the platform movement during the building process requires the designed hardware to ensure the repeatability between different layers which increases the overall cost of the system. Zabti [32] carried out Pareto based Multi-objective function based optimization of STL process which has three objective functions. The goal is to find the optimum exposure time value by minimizing the cure depth, surface roughness and maximizing the mechanical strength. Lehtinen [33] developed a DMD based projection stereolithography and a computer code is written to control the entire manufacturing process. Gandhi et al. [34] analyze various optical scanning schemes used for MSL systems along with the proposed scheme via optical simulations and experiments. The mechanical design of the scanning mechanism is carried out to meet requirements of high speed and resolution. The system integration and investigation in process parameters is carried out and fabrication of large micro-component with high resolution is demonstrated. Campaigne III [35] developed projection stereolithography and material characterization of nanocomposites photopolymers was carried out. Valentincic et al. [36] conclude that DLP based stereolithography is used to reduce the build time and to increase the manufacturing accuracy. Compared to fused deposition modeling (FDM) machines, machines for DLP stereolithography are expensive and thus not available to a broad range of users as it is the case with FDM 3D printers. Luo et al. [37] developed desktop manufacturing system which can produce RP parts with good machining efficiency, but the surface roughness should be further improved. Ibrahim et al. [38] investigate the influence of process parameters which are layer thickness and exposure time on physical and mechanical properties of DLP structure.

Thus, by going through the aforementioned literature on SL systems, it is observed that most of researchers develop microstereolithography systems. The developed SL systems are either LCD based or DMD based. The disadvantages of LCD based SL systems are low pixel filling ratio, print – through errors occurs due to light that penetrates into already cured layers, unnecessary wavelengths cause inaccurate dimensions in the cured part. The advantages of DMD based SL systems are availability of UV compatibility, high modulation efficiency, high light transmission, high optical fill factor, low pitch size and pixel size. Both the developed SL systems i.e. LCD as well as DMD based mentioned in above

literature survey are very expensive, which are not affordable to common or medium sized industries or vendors who can build their prototypes with a cheaper cost. Therefore, development of a low cost SLA with better build speed is a goal of this research work.

The sub-section 2.1 of section 2 describes the developed low cost SLA in detail with specifications of the sub-systems, different softwares, photo-polymer and photo-initiator used in the apparatus. In sub-section 2.2 the absorbance spectrum of photo-curable resin and light beam spectrum of DLP projector are plotted. In sub-section 2.3 the slicing procedure of 3D CAD model into 2D slices is explained with the help of developed MATLAB code. The experimental results and discussions are given in section 3. Finally, the conclusions are drawn from experimental work in section 4.

## 2. EXPERIMENTAL SET UP

### 2.1 Stereolithography apparatus (SLA)

The stereolithography apparatus (SLA) is developed to produce highly precise, three-dimensional (3D) structures from broad selection of functional materials, especially photopolymer resin. The lay-out of the experimental set-up is shown in Figure 1 and the CAD model is shown in Figure 2. The developed stereolithography apparatus (SLA) utilizes focused light beam from DLP projector and then through the objective lens over the surface of a photo-curable resin, which undergoes photo-polymerization and forms solid structures. The lamp of the modified DLP projector works as light source and DMD chip in the DLP projector works as a dynamic pattern generator for this SLA. The colour wheel of the DLP projector is filtering most of the UV light out. But UV light is required for solidification of the photopolymer. Therefore, we had done changes in the colour wheel. The color wheel is a glass disc with several colored segments that spins while the projector is running to colorize the image. The projector actually requires it to run; when the color wheel is simply removed, the projector would not turn on the lamp. Therefore, only glass portion of the color wheel is removed so that maximum UV light should come out from the projector which is the requirement for solidification of liquid resin. After removing glass portion from the color wheel, the projector becomes black and white. Infocus make DLP projector with display resolution 1024×768 is used. The photograph of actual experimental set-up is shown in Figure 3.

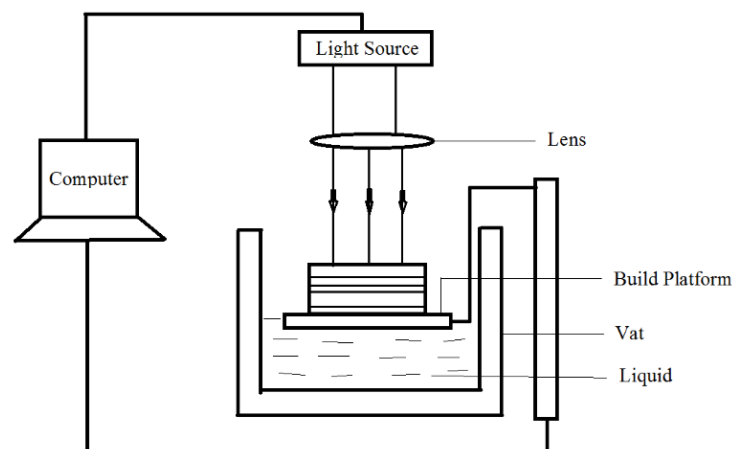
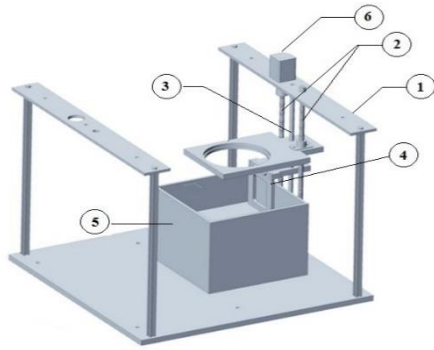
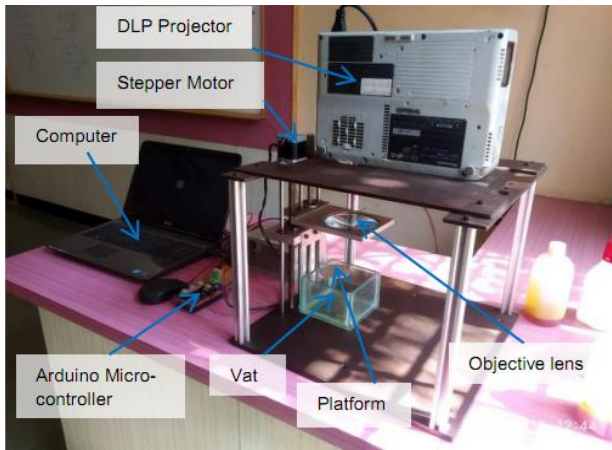


Figure 1. Lay-out of the experimental set –up



1-Frame, 2-Ball Screw, 3-Guide rod, 4-Z stage, 5-Resin Tank, 6-Stepper motor

**Figure 2.** CAD model of experimental set-up without DLP projector



**Figure 3.** Experimental set-up

The photopolymer used in this experimentation is polyethylene glycol di-acrylate with 2% Irgacure 784 as photo-initiator. The absorbance spectrum of the photopolymer is plotted and the maximum absorbance observed is in the range of 315 nm to 480 nm. The peak absorbance of polyethylene glycol di-acrylate matches with the peak intensity of light beam of DLP projector which is in the range of 400 nm – 570 nm. Therefore, polyethylene glycol di-acrylate is selected as photo-curable resin and cost of the same resin is also low as compared to other resins. From this data it is concluded that maximum UV light is required for solidification of the photopolymer. The NEMA 17 bipolar stepper motor with 0.9° step angle, 5% step accuracy, 5 mm shaft diameter is used to rotate the ball screw. The ball screw with nominal diameter 12 mm, pitch 2.0 mm, core diameter 10.084 mm and lead angle 3.04° is used for up and down motion of the Z-stage. The maximum speed of the stepper motor is 2344 rpm and holding torque is 4.8 kg-cm. The Creo 3.0 software is used for modeling of 3D CAD model. The 3D CAD model and STL file format in Creo 3.0 software is more compatible with developed MATLAB code for slicing of 3D CAD model as compared to other modeling softwares. Therefore, Creo 3.0 software is selected for 3D CAD modeling. A special MATLAB code is developed for slicing of the 3D CAD model and this sliced 3D CAD model is imported into the Creation Workshop software version 1.0.0.75 which is used to control the focusing time period of sliced images through DLP projector and focusing lens. The make of focusing lens is Optics and Allied Engineering Private Limited, Bangalore with 100 mm diameter and 100 mm focal length.

The Creation Workshop software also controls the motion of the Z-stage through Arduino MEGA 2560 micro- controller and NEMA 17 bipolar stepper motor. It also controls input parameters, such as layer thickness, motor movement speed, exposure time and settling period. These parameters make the equipment versatile and suitable for a wide range of different tasks. Finally, the different shape objects are built by curing the aforementioned photo-curable resin. The photographs of the build components are taken by the Amp Cam digital microscope with optimum resolution 640×480 and 5X digital zoom. The FARO Edge 3D scanner with the specifications ±25µm accuracy, 25µm repeatability, 115 mm depth of field, 80 mm effective scan width for near field, 2,000 scanning points per line, 40µm minimum point spacing, 280 frames/second scan rate and Class 2M laser is used to measure the dimensions of the build objects. Thus, a low cost, high build speed SLA is developed to fabricate 3D components.

In the Z- Stage, we have to control the linear movement of the platform with the help of stepper motor and ball screw. The stepper motors rotational motion is transformed in to linear motion with help of ball screw coupled with motor shaft. Arduino microcontroller is used for precise and accurate control the movement of the motion stage. The rotational movement of the stepper motor is controlled with the help of special Arduino program. The program mainly consists of various commands and statements to control the various parameters such as speed, time delay etc. Figure 4 shows the window of Arduino software in which the uploaded program is shown. The Arduino Micro-controller with stepper motor is interfaced with Creation Workshop Software to obtain desired motion of Z-stage.

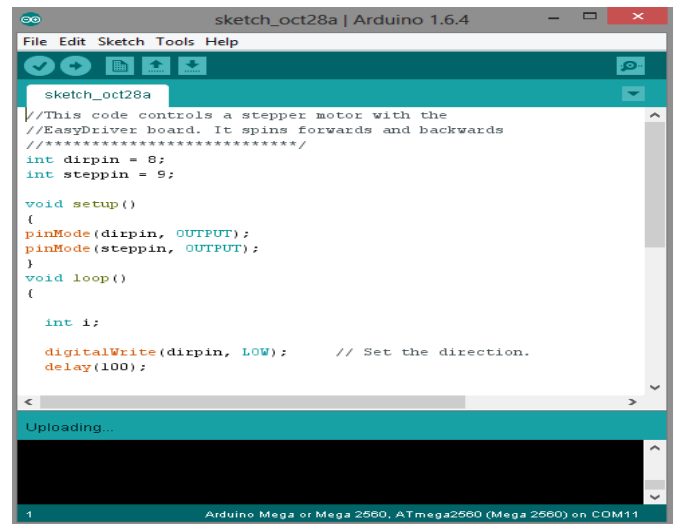


**Figure 4.** The program uploaded to the Arduino software

## 2.2 Spectrum study of photopolymer and DLP projector

The 3D object is built by focusing the light beam of DLP projector through objective lens on the z-stage platform. On the Z-stage platform a layer of liquid photopolymer of thickness equal to the slice thickness of CAD model is made available by lowering the platform with help of ball screw and stepper motor. Therefore, it is necessary to plot the absorbance spectrum of photopolymer from which we can conclude that what is value of wave length for peak absorbance. The Figure 5 shows the absorbance spectrum plot of photopolymer and it is observed that the peak absorbance is at wavelength 335 nm,

410 nm and 480 nm. Therefore, the focused light beam must have the peak wavelength in the range of 300 – 500 nm which is a UV light region.

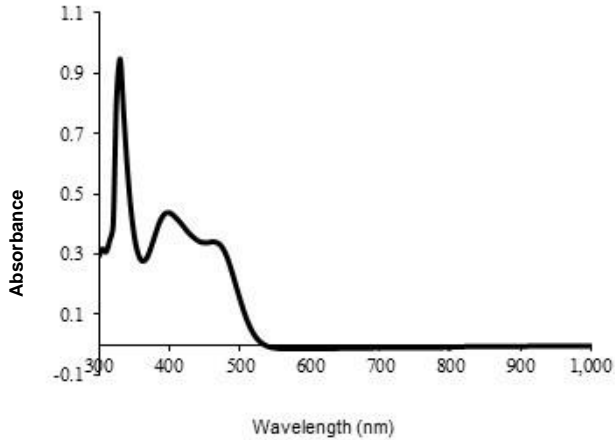


**Figure 5.** Absorbance spectrum of photopolymer

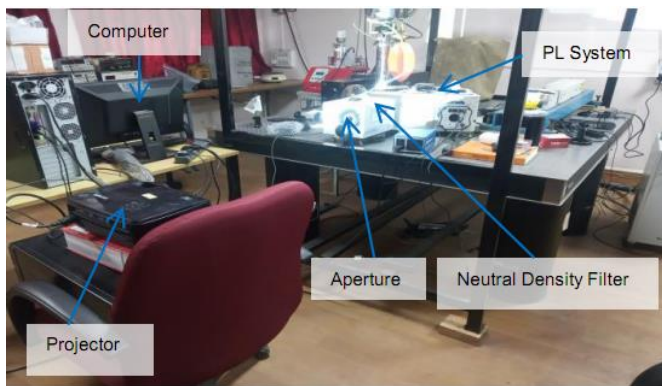


**Figure 6.** DLP projector light beam spectrum plotting set-up

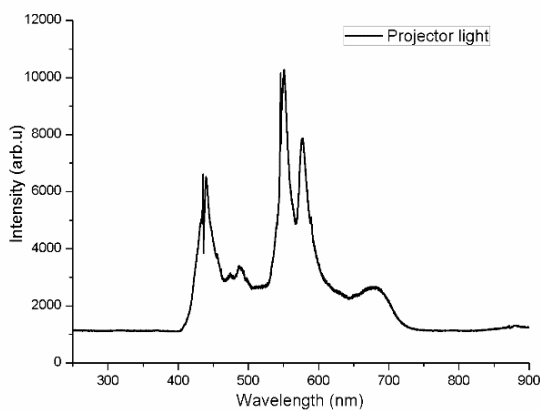


**Figure 7.** Light beam spectrum of DLP projector

The study of DLP light beam spectrum is done by using Horriba (model iHR320) light spectrometer. The Figure 6 shows the set-up for plotting the spectrum of DLP projector light beam. The light beam from the DLP projector is passed through the aperture then it passes through the neutral density filter. The neutral density filter removes the unwanted light rays. The spectrum is plotted for the light wavelength range of 250 – 900 nm. Finally, light beam passed into the photoluminescence (PL) system. The PL system consists of optical grating, mirror 1 and mirror 2 with CCD (closed circuit

device) camera. The measured spectrum data by PL system is collected by the computer. The Figure 7 shows the light beam spectrum obtained by above mentioned spectrometer. From light beam spectrum it is observed that the peak values are in the wavelength range of 400 nm – 570 nm. Therefore, the light beam of DLP projector is useful to cure the selected photopolymer as peak wavelength range matches with each other.

### 2.3 Slicing of 3D CAD model

Basically, the stereolithography equipment consists of a DLP projector, focusing lens, resin vat, a linear translation stage with a platform and a computer. Before the manufacturing can begin, some preparations must be done. First, the CAD model is sliced into horizontal cross-section images. These black and white images will be projected one by one onto the platform with resin layer. As there are different methods available to slice a CAD model without tessellation but slicing a triangulated mesh model is still the commonly used method in 3D printing caused by its format (i.e. STL) is widely adopted in software and machine. These different methods of slicing a 3D CAD models are Contour, Voxelization and Ray tracing [39]. The contour method is the traditional slicing process that generates the cross-sectional information by intersecting the input model with a set of horizontal planes. As the input model is tessellated into faces (e.g. triangles defined in the STL), the slicing operation is actually a number of face-plane intersections, each of which is a segment. In a layer, the intersection between the model and a slicing plane is one or more polygons (contours), which are constituted by the segments. The voxelization method creates a 3D array of voxels that can cover the whole volume of the input model, and then decides whether each voxel is inside or outside the model. The in/out determination is challenging, because the mesh is just a set of faces in the 3D space without the information of inside or outside. In ray-tracing method, 2D image is used and in/out for every pixel in a slice is determined similar to point-in-polygon testing. In this method testing can be done by casting a ray from each pixel to intersect with the model, and finding out if the ray reaches the interior or exterior of the model at a particular height. Out of the above three slicing technologies, the ray-tracing method is the fastest in most cases and it needs a moderate amount of memory for computation. It maintains a good balance between computation time and memory space. It would be optimal if the intersection problem can be handled without creating other problems. Therefore, due to these advantages, the ray-tracing method is used for development of a special MATLAB code for slicing of 3D CAD model in this research work.

The STL file shown in Figure 8 was originally conceived by 3D Systems [40] and it opened the door for rapid prototyping and manufacturing market by allowing CAD data to be used in STL systems. The file consists of an unordered list of triangular facets that represent the outside skin of a part. The triangular facets are described by a unit normal vector and a set of X, Y, Z coordinates for each of the three vertices. The unit vectors indicate the outside of the part. Since the STL model consists of triangular facets, it is an approximate model of the accurate CAD data. Regardless of being an imprecise model, STL has become the standard used by most CAD and RP systems. STL is a simple solution for representing 3D CAD data and it provides small and accurate files for data transfer for specific shapes [41, 42]. There are two formats for STL file:

ASCII and Binary which are shown in Figure 9 and Figure 10 respectively. Binary files are smaller and more compact. Hence, they are more common. After generating the STL file of the 3D CAD model then it is necessary to slice the model into a number of horizontal cross-section images. The 3D CAD model of the object which is to be built by using stereolithography process is developed with the help of CREO 3.0 software. Then it is saved in STL file format using the same software. The Figure 11 shows the 3D CAD model in STL file format.

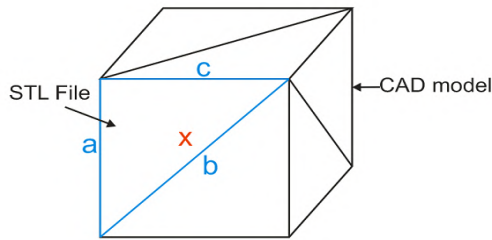


**Figure 8.** Standard Tessellation Language (STL) file and CAD model [42]

```

solid name

facet normal ni nj nk
  outer loop
    vertex v1x v1y v1z
    vertex v2x v2y v2z
    vertex v3x v3y v3z
  endloop
endfacet

endsolid name

```

**Figure 9.** ASCII STL file format [42]

```

UINT8[80] - Header
UINT32 - Number of triangles

foreach triangle
  REAL32[3] - Normal vector
  REAL32[3] - Vertex 1
  REAL32[3] - Vertex 2
  REAL32[3] - Vertex 3
  UINT16 - Attribute byte count
end

```

**Figure 10.** Binary STL file format [42]

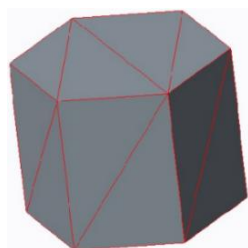


**Figure 11.** 3D CAD model in STL file format

Thus, a special MATLAB code is developed by using ray tracing method and by using this code, the 3D CAD model is sliced into a number of layers as shown in Figure 12. The Figure 13 (a) and (b) shows a single sliced layer in MATLAB software window. Then these sliced layers are imported in Creation Workshop software and focused one by one at required time interval with the help of DLP projector through objective lens on the Z- stage platform and finally the 3D object is built.

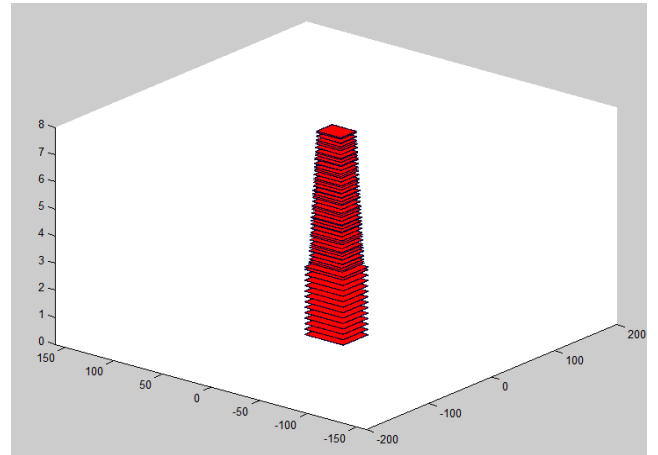
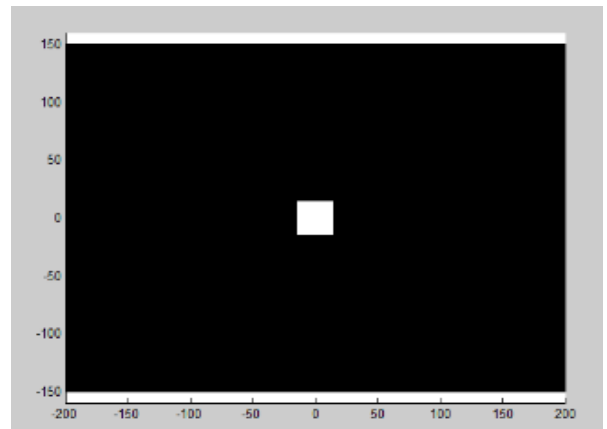
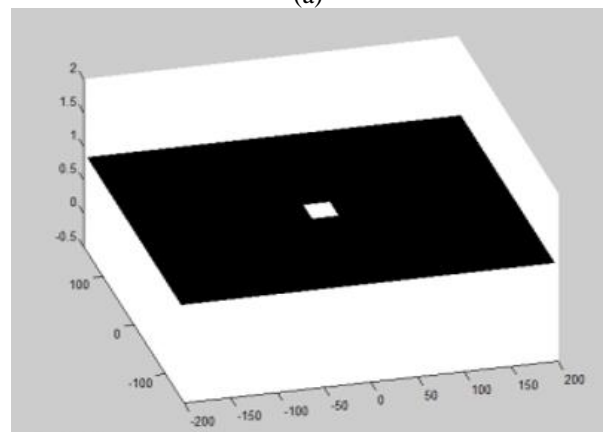


**Figure 12.** Sliced 3D CAD model



(a)



(b)

**Figure 13.** 2D Slices in MATLAB window

### 3. RESULTS AND DISCUSSIONS

The experiments are performed with hexagonal cross-

section and pyramid objects with 0.1 mm curing depth along Z – axis. The trials are performed with different exposure time and settling period. The exposure time is varied from 10 seconds to 1 second and it is observed that the objects are best cured for 2 seconds curing period. The experimental test data for hexagonal cross-section and pyramid objects are given in Table 1 and Table 2 respectively. The CAD model of the hexagonal prism is shown in Figure 14 and scanned image of build hexagonal prism by FARO Edge 3D scanner is shown in Figure 15. The built hexagonal prism is shown in Figure 16 (a) and (b). The Figure 17 shows the measurements of dimensions of hexagonal prism by FARO Edge 3D scanner. The Figure 18 shows the CAD model of pyramid and Figure 19 shows the built pyramid. The scanned image of built pyramid by FARO Edge 3D scanner is shown in Figure 20 and the measurement of dimensions of pyramid by FARO Edge 3D scanner are shown in Figures 21-23. The pyramid object with 120 numbers of layers with 12 mm dimension along Z-axis is built. The maximum area 18 mm x 16 mm of pyramid object along X-Y plane is cured. For commercial SLA machines resolution in Z-axis is in between 0.01 to 0.25 mm. The resolution along Z-axis of 0.25mm creates a fairly coarse surface for medium sized parts, but for larger models, the layer steps are not too noticeable due to the relative size of larger parts. A resolution of 0.1mm provides a more favorable surface finish for medium and small parts. Therefore, experiments are performed with 0.1 mm curing depth along Z-axis. The maximum exposure area obtained is 55mm x 45mm. It is observed that as the curing time decreases the percentage error between the 3D CAD model dimensions and built dimensions are also decreases. The maximum and minimum percentage errors for hexagonal cross-section object are 9.43 and 2.0 respectively. The maximum and minimum percentage errors for pyramid object are 4.44 and 0.93 respectively. The minimum percentage error is observed for 2 seconds curing period. The dimensions of the built components are measured by FARO Edge 3D scanner with  $\pm 25\mu\text{m}$  accuracy. Creation Workshop software Version 1.0.0.75 is used: (i) to control the Z-stage motion, (ii) to control the focusing time of sliced images and settling time. The resolution of the built components depends upon Software Imposed Parameters (SIP) and SL Process Parameters (PP). The Software Imposed Parameters (SIP) are line width compensation, .stl file resolution, layer thickness, z compensation, and stereolithography grid. The SL Process Parameters (PP) consists of light beam size and intensity, light beam focus depth, and layer thickness [43].

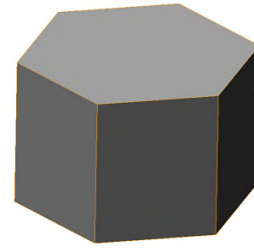


Figure 14. CAD model of hexagonal prism

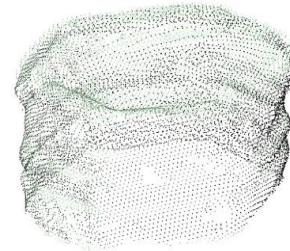


Figure 15. Scanned image of build hexagonal prism

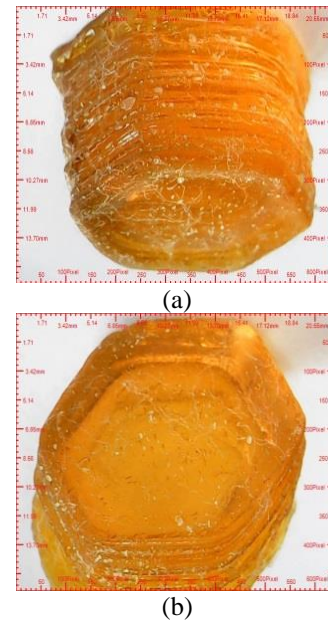


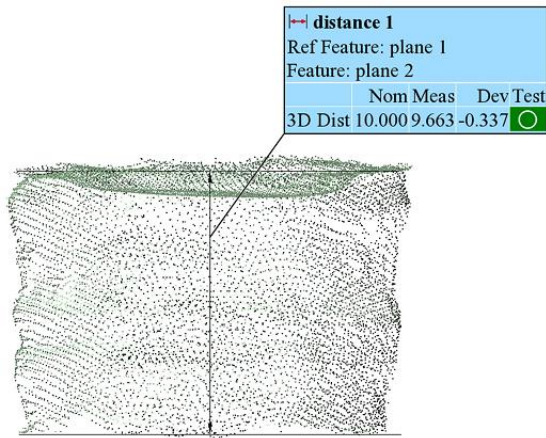
Figure 16. Built hexagonal prism

Table 1. Hexagonal prism experimentation data

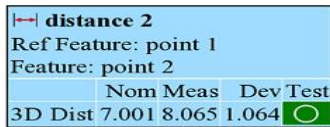
Object Cross-section	Measuring Scale	Dimensions (mm)			Layer thickness (mm)	No. of layers	Exposure time (sec.)	Settling Period (sec.)	Build time (sec.)
		x	y	z					
Hexagon (7 mm side)	CAD Model	14	14	10	0.1	100	2	3.5	546.5
	Built object	15.32	14.28	9.66					
	% Error	9.43	2.0	3.4					

Table 2. Pyramid experimentation data

Object Cross-section	Measuring Scale	Dimensions (mm)			Layer thickness (mm)	No. of layers	Exposure time (sec.)	Settling Period (sec.)	Build time (sec.)
		x	y	z					
Pyramid	CAD Model	18	16	12	0.1	120	2	3.5	656.5
	Built object	17.20	16.15	10.85					
	% Error	4.44	0.93	2.33					



(a)



(b)

Figure 17. Measurement of height and side of hexagonal prism

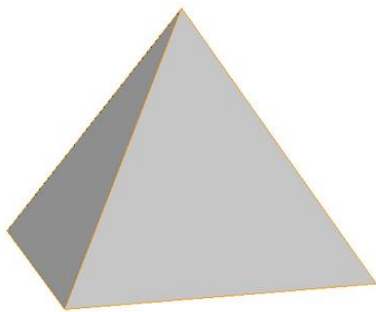


Figure 18. CAD Model of pyramid



Figure 19. Built pyramid

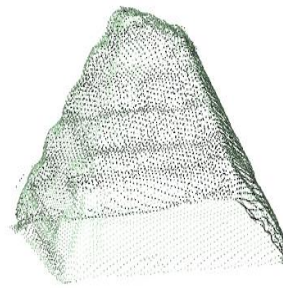


Figure 20. Scanned Image of build pyramid

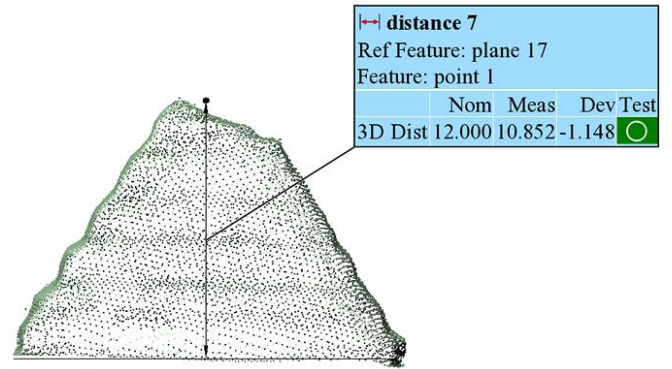


Figure 21. Height measurement of build pyramid

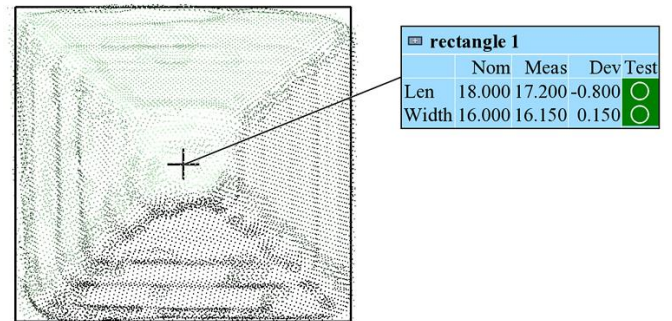


Figure 22. Base measurement of pyramid

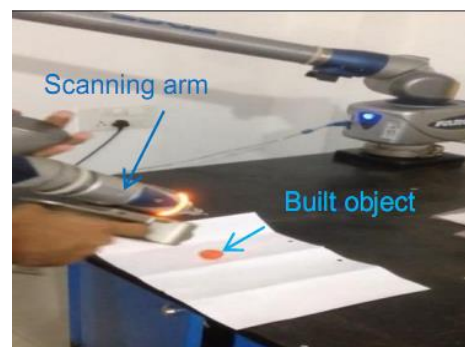


Figure 23. Faro edge 3D scanner

#### 4. CONCLUSIONS

A low cost stereolithography apparatus (SLA) has been developed with DLP projector as a UV light source. The overall cost of the developed SLA is very low as compared to the present commercial SLA available. Therefore, the build cost of the fabricated objects is reduced due to developed low

cost SLA. The optimum curing period per layer is two seconds per layer as the percentage error is minimum for two seconds curing period. Therefore, build speed obtained is two seconds per layer which is remarkable compared with present SLA. The dimensional accuracy of fabricated objects is also satisfactory as the maximum and minimum percentage error is 9.43 and 0.93 respectively which is acceptable comparing with the results available in the literature [33, 36]. The dimensional percentage error is decreased as the curing period or image focusing period is reduced. The pyramid object with maximum 120 numbers of layers with 12 mm dimension along Z-axis is built in 11 minutes. The maximum exposure area obtained which can be cured in X-Y plane is 55 mm x 45 mm. The resolution of the build objects in X-Y plane is 23 microns which is resolution of sliced image focused from DLP projector and Z-stage resolution is 0.1 mm. The advantages of the developed SLA are low build cost, high fabrication speed, excellent resolution in X-Y plane, low resin cost etc. The limitations are low dimensional accuracy, poor resolution of the fabricated objects along Z-stage. The future scope of the work is to introduce the dimensional error correction model in the experimentation to minimize the percentage errors of the build objects. Another future scope is to perform the experiments with values lower than 0.1 mm curing depth so that resolution of build objects along Z- stage will be improved.

#### ACKNOWLEDGMENT

The authors are thankful to the Board of Colleges and University Development (BCUD) of Savitribai Phule Pune University, Pune for funding this research project under the grant number OSD/BCUD/360/122. The authors are also thankful to Dr. S. H. Gawande Professor, M.E.S. College of Engineering, Pune for technical support and Management, Principal Dr. R. V. Patil of Pune District Education Association's College of Engineering, Manjari (Bk.), Pune for permitting to carry out this research work.

#### REFERENCES

- [1] Wilson, J., Hawkes, J.F.B. (1987). *Lasers, Principles and Applications*. Prentice Hall, New York.
- [2] Gibson, I., Rosen, D.W., Stucker, B. (2009). *Additive manufacturing technologies: Rapid Prototyping to Direct Digital Manufacturing*. Springer, New York.
- [3] Chua, C.K., Leong, K.F., Lim, C.S. (2003). *Rapid Prototyping – Principles and Applications*. World Scientific Publishing, Singapore.
- [4] Gibson, I. (2006). Rapid prototyping from product development to medicine. *Virtual and Physical Prototyping*, 1(1): 31-42. <http://dx.doi.org/10.1080/17452750500271298>
- [5] Bidanda, B., Bartolo, P.J. (2008). *Virtual prototyping and Bio-manufacturing in medical applications*. Springer, New York. <http://dx.doi.org/10.1007/978-0-387-68831-2>
- [6] Fouassier, J. (1995). *Photoinitiation, Photopolymerization, and Photocuring: Fundamentals and Applications*. Hanser.
- [7] Fujimasa, I. (1996). *Micromachines: A New Era in Mechanical Engineering*. Oxford University Press.
- [8] Ventura, S.C., Narang, S.C., Sharma, S., Stotts, J., Liu, C., Liu, S., Ho, L.H., Annavajjula, D., Lombardi, S.J., Hardy, A., Mangaudis, M., Chen, E., Groseclose, L. (1996). A new SFF process for functional ceramic components. *Proceedings of the Solid Freeform Fabrication*, pp. 327-334.
- [9] Bertsch, A., Zissi, S., Jezequel, J., Corbel, S., André, J. (1997). Microstereolithography using liquid crystal display as dynamic mask-generator. *Microsystems Technologies*, 3(2): 42-47. <https://doi.org/10.1007/s005420050053>
- [10] Maruo, S., Kawata, S. (1998). Two-photon-absorbed near-infrared photopolymerization for three-dimensional microfabrication. *Journal of Microelectromechanical Systems*, 7(4): 411-415. <http://dx.doi.org/10.1109/84.735349>
- [11] Young, J.S., Fox, S.R., Anseth, K.S. (1999). A novel device for producing three dimensional objects. *Journal of Manufacturing Science & Engineering*, 121(3): 474-477. <http://dx.doi.org/10.1115/1.2832705>
- [12] Ikuta, K., Hirowatari, K. (1993). Real three-dimensional microfabrication using stereolithography and metal mold. *Proceedings of IEEE International Workshop on Micro Electro Mechanical Systems (MEMS'93)*, pp. 42-47.
- [13] Monneret, S., Le, G., Bade, H., Devaux, V., Mosset, F., Lantz, A. (2002). Dynamic UV microstereolithography. *Applied Physics*, 6(3): 213-218. <http://dx.doi.org/10.1051/epjap:2002094>
- [14] Sun, C., Zhang, X. (2002). Experimental and numerical investigations on Microstereolithography of ceramics. *Journal of Applied Physics*, 92(8): 4796. <http://dx.doi.org/10.1063/1.1503410>
- [15] Bertsch, A., Jiguet, S., Renaud, P. (2003). Microfabrication of ceramic components by microstereolithography. *Journal of Micromechanics and Microengineering*, 14(2): 197-203. <http://dx.doi.org/10.1088/0960-1317/14/2/005>
- [16] Huang, Y.M., Jiang, C.P. (2003). Numerical analysis of a mask type stereolithography process using a dynamic finite element method. *The International Journal of Advanced Manufacturing Technology*, 21(9): 649-655. <http://dx.doi.org/10.1007/s00170-002-1388-x>
- [17] Lee, I.H., Cho, D.W., Lee, E.S. (2004). Development of microstereolithography systems for the fabrication of three-dimensional micro-structure. *Journal of Korean Society Precision Engineering*, 21(2): 29-36. <https://doi.org/10.1007/s00170-008-1461-1>
- [18] Jiang, C.P., Jeng, J.Y., Huang, Y.M., Tsai, M.J. (2005). Development of masked photo-polymerization rapid prototyping system using liquid crystal display panel. *Journal of the Chinese Institute of Industrial Engineers*, 22(1): 76-81. <http://dx.doi.org/10.1080/10170660509509279>
- [19] Lee, D., Miyoshi, T., Takaya, Y., Ha, T. (2006). 3D microfabrication of photosensitive resin reinforced with ceramic nanoparticles using LCD micro stereolithography. *Journal of Laser Micro/Nano Engineering*, 1(2): 142-148.
- [20] Deshmukh, S.P., Dubey, S., Gandhi, P.S. (2006). Optical analysis of scanning micro stereolithography systems. *Micromachining and Microfabrication Process Technology XI, Proceedings*, 61090C. <http://dx.doi.org/10.1117/12.645856>
- [21] Limaye, A.S. (2007). Multi-objective process planning method for mask projection stereolithography. PhD

- dissertation, Georgia Institute of Technology.
- [22] Hadipoespito, G.W., Yang, Y., Choi, H., Ning, G., Li, X. (2003). Digital micromirror device based microstereolithography for micro structures of transparent photopolymer and nanocomposites. Department of Mechanical Engineering University of Wisconsin-Madison, Madison, WI 53706.
- [23] Singhal, S.K., Jain, P.K., Pandey, P.M. (2008). Adaptive slicing for SLS prototyping. *Computer-Aided Design and Applications*, 5(1-4): 412-423. <http://dx.doi.org/10.3722/cadaps.2008.412-423>
- [24] Choi, J., Kang, H.W., Lee, I.H., Ko, T.J. (2009). Development of micro-stereolithography technology using a UV lamp and optical fiber. *International Journal of Advance Manufacturing Technology*, 41: 281-286. <https://doi.org/10.1007/s00170-008-1461-1>
- [25] Zhao, X. (2009). Process planning for thick-film mask projection micro-stereolithography. PhD thesis, Georgia Institute of Technology.
- [26] Vatani, M., Rahimi, A.R., Brazandeh, F., Sanatinezhad, A. (2009). An enhanced slicing algorithm using nearest distance analysis for layer manufacturing. *World Academy of Science, Engineering and Technology*, 3(1): 74-79. <https://doi.org/10.5281/zenodo.1082905>
- [27] Deshmukh, S.P., Gandhi, P.S. (2009). Optomechanical scanning systems for microstereolithography (MSL): Analysis and experimental verification. *Journal of Materials Processing Technology*, 209(3): 1275-1285. <http://dx.doi.org/10.1016/j.jmatprotec.2008.03.056>
- [28] Choi, J.W., Wickera, R., Leeb, S.H., Choi, K.H., Had, C.S., Chung, I. (2009). Fabrication of 3D biocompatible/biodegradable micro-scaffolds using dynamic mask projection microstereolithography. *Journal of Materials Processing Technology*, 209(15-16): 5494-5503. <http://dx.doi.org/10.1016/j.jmatprotec.2009.05.004>
- [29] Gandhi, P.S., Deshmukh, S.P. (2009). A 2D optomechanical focused laser spot scanner: Analysis and experimental results for microstereolithography. *Journal of Micromechanics and Microengineering*, 20(1): 15-35. <http://dx.doi.org/10.1088/09601317/20/1/015035>
- [30] Itoga, K., Kobayashi, J., Yamato, M., Okano, T. (2010). Development of microfabrication technology with maskless photolithography device using LCD projector. *Journal of Robotics and Mechatronics*, 22(5): 608-612. <http://dx.doi.org/10.20965/jrm.2010.p0608>
- [31] Zhou, C., Chen, Y. (2011). Additive manufacturing based on optimized mask video projection for improved accuracy and resolution. *Proceedings of NAMRI/SME*, 14(2): 107-118. <http://dx.doi.org/10.1016/j.jmapro.2011.10.002>
- [32] Zabti, M.M. (2012). Effects of Light Absorber on micro stereolithography parts. PhD thesis, School of Mechanical Engineering, The University of Birmingham, Edgbaston, Birmingham.
- [33] Lehtinen, P. (2013). Projection microstereolithography equipment. MS thesis, School of Science, Aalto University.
- [34] Gandhi, P.S., Deshmukh, S.P., Ramtekkar, R., Bhole, K., Baraki, A. (2013). "On-axis" linear focused spot scanning microstereolithography system: optomechtronic design, analysis and development. *Journal of Advanced Manufacturing Systems*, 12(01): 43-68. <http://dx.doi.org/10.1142/S0219686713500030>
- [35] Campaigne III, E.A. (2014). Fabrication and Characterization of Carbon Nanocomposite Photopolymers via Projection Stereolithography. MS Thesis, Virginia Polytechnic Institute and State University, USA.
- [36] Valentincic, J., Perosa, M., Jerman, M., Sabotin, I., Lebar, A. (2017). Low cost printer for DLP stereolithography. *Journal of Mechanical Engineering*, 63(10): 559-566. <http://dx.doi.org/10.5545/sv-jme.2017.4591>
- [37] Luo, R.C., Tzou, J.H. (2010). Development of a LCD Photomask Based Desktop Manufacturing System. Motion Control, Federico Casolo (Ed.), ISBN: 978-953-7619-55-8, <http://dx.doi.org/10.1109/TIE.2008.922603>
- [38] Ibrahim, A., Saude, N., Ibrahim, M. (2017). Optimization of process parameter for digital light processing (DLP) 3D printing. *Proceedings of Academics World 62nd International Conference*, Seoul, South Korea, 18th -19th April 2017, pp. 11-14.
- [39] Kwok, T.H. (2017). Comparing slicing technologies for digital light processing printing. ASME, Department of Mechanical, Industrial and Aerospace Engineering Concordia University Montreal, Canada, 19(4): 044502. <http://dx.doi.org/10.1115/1.4043672>
- [40] 3D Systems (1988). *Stereolithography Interface Specification*, Inc.
- [41] Chua, C., Leong, K., Lim, C. (2010). *Rapid Prototyping: Principles and Applications*. Third edition, World Scientific.
- [42] Jacobs, P., Reid, D. (1992). *Rapid Prototyping and Manufacturing: Fundamentals of Stereolithography*. Society of Manufacturing Engineers.
- [43] Sager, B., Rosen, D. (2002). *Stereolithography Process Resolution*, The George W. Woodruff School of Mechanical Engineering Georgia Institute of Technology Atlanta, USA.

## NOMENCLATURE

3D	three dimensional
AM	additive manufacturing
CAD	computer aided design
CAM	computer aided manufacturing
DLP	digital light processing
DMD	digital micro-mirror device
LCD	liquid crystal display
MEMS	micro-electro-mechanical systems
MSL	microstereolithography
PL	photoluminescence
RP	rapid prototyping
SL	stereolithography
SLA	stereolithography apparatus
STL	standard tessellation language
UV	ultra-violet